Limited glacial erosion during the last glaciation in mid-latitude cirques (Retezat Mts, Southern Carpathians, Romania)

Zsófia Ruszkiczay-Rüdiger, Zoltán Kern, Petru Urdea, Balázs Madarász, Regis Braucher

Geomorphology 384 (2021) 107719

Contents lists available at ScienceDirect

Geomorphology

journal homepage: www.elsevier.com/locate/geomorph

Limited glacial erosion during the last glaciation in mid-latitude cirques (Retezat Mts, Southern Carpathians, Romania)

Zsófia Ruszkiczay-Rüdiger [a,*], Zoltán Kern [a], Petru Urdea [b], Balázs Madarász [c], Régis Braucher [d], ASTER Team [d,1]

[a] Institute for Geological and Geochemical Research, Research Centre for Astronomy and Earth Sciences, Budaörsi út 45, 1112 Budapest, Hungary
[b] Department of Geography, West University of Timisoara, Romania
[c] Geographical Institute, Research Centre for Astronomy and Earth Sciences, Budaörsi út 45, 1112 Budapest, Hungary
[d] Aix-Marseille Univ., CEREGE, CNRS-IRD-Collége de France-INRAE BP 80, 13545 Aix-en-Provence Cedex 4, France

ARTICLE INFO

Article history:
Received 28 January 2021
Received in revised form 24 March 2021
Accepted 25 March 2021
Available online 6 April 2021

Keywords:
Cosmic ray exposure dating
Inheritance
Glacial erosion
Glacial cirques
Cosmogenic ^{10}Be
LGM
Carpathians
Deglaciation

ABSTRACT

The studied dataset from the Southern Carpathians permitted the quantification of a considerable amount of inherited ^{10}Be in the glacial boulders and bedrock samples in the cirque area. The samples from the glacial phases of largest extension display no signs of significant inheritance, and enabled the establishment of a deglaciation chronology in the southern valleys of the Retezat Mts. The timing of the maximum glacier extent ($20.6^{+0.8}/_{-1.3}$ ka) coincided with the Last Glacial Maximum, which was followed by five deglaciation phases during the Lateglacial having partly overlapping ages due to fast glacier retreat (at $18.4^{+0.7}/_{-1.1}$ ka; 16.9 ± 0.9 ka, $15.8^{+0.9}/_{-0.6}$ ka, $15.6^{+0.8}/_{-0.8}$ ka and 14.4 ± 0.5 ka) but could be distinguished by the position of their terminal moraines.
The currently available geochronological data do not support the assumption of any major glacial re-advance after Greenland Stadial 2.1a in the Retezat Mts.
Given the lack of independent geochronological data, the amount of inherited cosmogenic nuclides is tentatively estimated by accepting the youngest cosmic ray exposure age(s) as the time of moraine deposition and abandonment by the glacier. The calculated amount of inherited ^{10}Be enables the estimation of a glacial erosion depth of 1.1–1.6 m for the bedrock samples and 1.4–1.8 m for the glacial boulders. The duration of the ice-covered and ice-free periods was adjusted in relation to independent paleoenvironmental and paleoclimatological data. The glacial denudation rate in the cirques was estimated at 19–28 mm/kyr and 24–33 mm/kyr for bedrock and boulders, respectively.
The limited glacial erosion in the cirques during the last glaciation is attributed to frozen-bed conditions with no considerable glacial deepening during the more extended glacial phases. Only when warming led to the retreat of the glaciers to their cirques, they become steeper and shift to being warm-based and thus more erosive. However, the limited time spent under these conditions appears to be too short to remove material from the cirque floors in sufficient depth (>3 m) to reset the cosmogenic clock. This suggests that the development of the cirques must have taken place during several subsequent glacial phases, providing an indirect confirmation of repeated Quaternary glaciations in the Retezat Mts.

1. Introduction

Mid-latitude mountain landscapes bear the unequivocal signs of effective erosion by glaciers during the Quaternary glaciations. Glacial cirques, U-shaped troughs, stoss-and-lee landforms (or roches moutonées), whalebacks and striated rock surfaces are typical macro- and mesoscale landforms shaped by past glacial erosion (Hugget, 2007). Part of the eroded material is deposited in the form of lateral and terminal (or frontal) moraine ridges in the ablation zone, at the sides and termination of the glacier tongues. Push moraines can develop during glacier advance, while successive build-up of moraines at stationary glacier margins has also been widely reported (Benn and Evans, 2010; Evans, 2014), both indicating the termination of the glacier snout. These landforms and sediments can therefore serve as benchmarks in reconstructing the ice extent in previous glacial phases and from this to make inferences concerning the interpretation of paleoclimate – provided that the age of their stabilization could be determined (Florineth and Schlüchter, 1998; Benn and Evans, 2010; Lukas, 2006).

Over the last three decades, advances in Cosmic Ray Exposure (CRE) dating methods using in situ produced ^{10}Be as a single nuclide or in combination with ^{26}Al or ^{14}C in quartz and ^{36}Cl in carbonates have enabled the direct age determination of glacial landforms, thereby revolutionizing our knowledge of glacial chronologies worldwide (Ivy-Ochs et al., 1996; Balco, 2011, 2020; Shakun et al., 2015). Dedicated samples originate from large moraine boulders or glacially scoured barren bedrock surfaces (Heyman et al., 2016; Fabel and Harbor, 1999; Jansen

* Corresponding author.
E-mail address: rrzsofi@geochem.hu (Z. Ruszkiczay-Rüdiger).
[1] Didier Bourlès, Georges Aumaître, Karim Keddadouche.

https://doi.org/10.1016/j.geomorph.2021.107719

et al., 2019; Prud'homme et al., 2020). The main geological factors that may lead to erroneous inferred ages are (1) exposure prior to glaciation and (2) incomplete exposure due to post-depositional shielding or denudation. In case of (1), the presence of certain amount of "inherited" cosmogenic nuclide inventory leads to inferred exposure ages that exceed the age of deposition. In scenario (2), shielding from cosmic rays by overburden or erosional loss can yield to a reduced amount of cosmogenic nuclides, and thus to apparent exposure ages which underestimate the deposition age (Heyman et al., 2011; Applegate et al., 2012).

The possibility of the presence of inherited cosmogenic nuclides was suggested in single-nuclide studies, in which the apparent CRE ages for a coherent landform tend to be biased towards greater ages (Harrison et al., 2010; Applegate et al., 2012). Several studies have found that nuclide abundances in glacially polished surfaces are considerably higher than in nearby glacially transported boulders or moraines (Briner and Swanson, 1998; Bierman et al., 1999; Briner et al., 2006; Crest et al., 2017; Jansen et al., 2019) or inversely, the cosmogenic nuclide concentrations of the glacially transported boulders exceeded that of the polished bedrock (Prud'homme et al., 2020). In other cases, an independent age control revealed that apparent exposure ages inferred from the cosmogenic nuclide concentrations tended to overestimate the true age of deglaciation, suggesting the probable presence of cosmogenic nuclide inheritance (Clark et al., 1995; Briner et al., 2016; Wirsig et al., 2017).

Several studies have suggested that the existence of cosmogenic nuclides accumulated in bedrock before the last glaciation is indicative of limited glacial erosion on high elevation plateaus (Stroeven et al., 2002; Briner et al., 2006; Bierman et al., 2015, Margreth et al., 2016; Young et al., 2018; Jansen et al., 2019). Some studies have also revealed that in mountain glaciations the glacial denudation of the cirques might have also been limited during the last glacial phase (Delmas et al., 2008; Crest et al., 2017; Valletta et al., 2017; Wirsig et al., 2017; Barr et al., 2019; Prud'homme et al., 2020).

If the inherited portion of the cosmogenic nuclide inventory can be estimated, it can be used for the quantification of the amount and/or rate of subglacial erosion (Fabel et al., 2004; Briner et al., 2006, 2016; Margreth et al., 2016; Crest et al., 2017; Knudsen and Egholm, 2018; Corbett et al., 2019; Jansen et al., 2019) or to reveal repeated phases of glacier advance and retreat (Bierman et al., 1999; Goehring et al., 2011; Schaefer et al., 2016; Crest et al., 2017; Wirsig et al., 2017).

The presented research aims at improving our knowledge of the deglaciation chronology of the Southern Carpathians via the ^{10}Be CRE dating of glacial landforms in the southern valleys of the Retezat Mts. The new dataset is compared to the published data from the northern valleys (Reuther et al., 2007; Ruszkiczay-Rüdiger et al., 2016). In the cirque area, where the ^{10}Be concentrations of the samples provide exceptionally old apparent exposure ages, the inherited ^{10}Be inventory in the bedrock and boulder surfaces could be estimated. The calculated amount of inherited ^{10}Be is then used for the estimation of the depth of glacial erosion and the glacial erosion rate during the last glaciation.

2. The study area

2.1. The topography and climate of the Southern Carpathians

The Carpathians form a mountain loop around the Pannonina Basin in Central Europe between the Mediterranean to the south, Alpine areas to the west and the Eastern European lowlands to the north and east (Fig. 1). The ~300 km long, E-W trending Southern Carpathians (~45.2–45.6° northern latitude) have the highest average elevation with 10 peaks culminating above 2500 m asl. Glacially sculpted landscapes are typical above ~1100 m above sea level (asl) in the highest mountains (Urdea, 2004; Urdea et al., 2011). Due to the continental climate and relatively low elevation of the range, glaciation was patchy and consisted primarily of glaciated cirques and plateaus, with valley glaciers restricted to the mountain ranges and not extending into the forelands (Urdea, 2004; Urdea et al., 2011; Mîndrescu et al., 2010; Popescu et al., 2017). Currently the area is ice-free. The altitude of the +2 °C annual isotherm is located at about 1600 m, while the −2 °C annual isotherm enclose only the highest massifs above ~2100 m asl (Micu et al., 2015). The annual precipitation increases from 500 to 800 mm in the foothill areas to 900–1300 mm above 800 m asl (Micu et al., 2015). The south-western slopes of the Retezat Mts are receiving more than 1000–1100 mm of precipitation yearly. In the Southern Carpathians winter precipitation usually falls in solid form above an elevation of ~1000 m. The season with continuous snow cover starts in mid-October and the snow melts between end of April and mid-June (Micu et al., 2015). Snowpack could be continuously present on ground up to 200–250 days/year in the alpine belt (Micu, 2009; Voiculescu and Ardelean, 2012).

Fir-spruce and fir-spruce-birch forest is typical under ~1600 m and densely growing dwarf pines in the ~1600–1800 m asl elevation range. Alpine meadows with patches of dwarf pines dominate the landscape in the ~1800–2200 m asl elevation range, while blockfields and rocky slopes are typical in the highest elevation belt.

2.2. The glacial landscape of the Retezat Mountains

The Retezat Mountains are in the western part of the Southern Carpathians with the highest peaks exceeding 2500 m asl (Fig. 1). They are characterised by the highest percentage of formerly glaciated areas (26.8%) and the lowest mean elevation of terminal moraines of the local Maximum Ice Extent (MIE) in the range (1100–1200 m asl; Urdea and Reuther, 2009).

In the Retezat Mts glacial cirques formed in every aspect around a central plateau and a main ridge. The cirques have their outflow through U-shaped glacial troughs descending in each direction (Urdea, 2000). The complex cirques of the Lăpuşnicu–Judele–Bucura system are carved into the southern side of the main ridge hosting the highest peaks (>2300 m asl). The main valley of this system (Lăpuşnicu Mare) accommodated the largest, ~16 km long glacier of the Southern Carpathians (Urdea, 2004). The present study aims at the age determination of glacial landforms in this valley system (Figs. 1, 2). Considering the mainly granitic lithologies of almost the entire area (Berza et al., 1994), time constraints of the local MIE and the following deglaciation phases can be provided by CRE dating using in situ produced cosmogenic ^{10}Be.

Another characteristic feature is the presence of two, 300–1200 m wide and flat-topped ridges extending south from the main ridge, which occupy an elevation range of 2000–2200 m asl, with an overall dip towards the south (Radeş-Zlata and Slaveiu plateaus; Fig. 2). Plateaus at 1800–2200 m asl are typical in the Southern Carpathians and are remnants of a formerly more extended peneplain called the Borăscu surface (Urdea et al., 2011). The plateaus are surrounded by glacial cirques with steep walls, and were home to ice fields during the most extended glacial phases, similarly to the neighbouring Godeanu Mts (Niculescu, 1965; Urdea et al., 2011; Ruszkiczay-Rüdiger et al., 2018; Ignéczi and Nagy, 2016) (Figs. 1, 2).

The cirques are typically wide and shallow, with two characteristic levels: a higher at ~2100–2200 m, and a lower at ~2000 m. Along the plateau edges cirques developed with cirque floors down to ~1800 m. The cirque-floor elevations of the southern valley heads are at similar elevation or somewhat above that of the cirque floors on the northern side of the range. The cirque floors are frequently occupied by glacial lakes dammed by bedrock steps and/or terminal moraines (Figs. 2, 3). In the U-shaped valleys, several lateral and terminal moraines have been described and mapped (Urdea, 2000). In the lower valley sections, moraines are more difficult to recognise due to their older age – which means there has been more time for their destruction by erosion – and also due to more dense vegetation. In this study the succession of terminal moraines in the Lăpuşnicu–Judele–Bucura valley system has been interpreted in a morphostratigraphic framework (Hughes et al., 2005), providing a solid basis for a geochronological study using the cosmogenic radionuclide (CRN) ^{10}Be. They

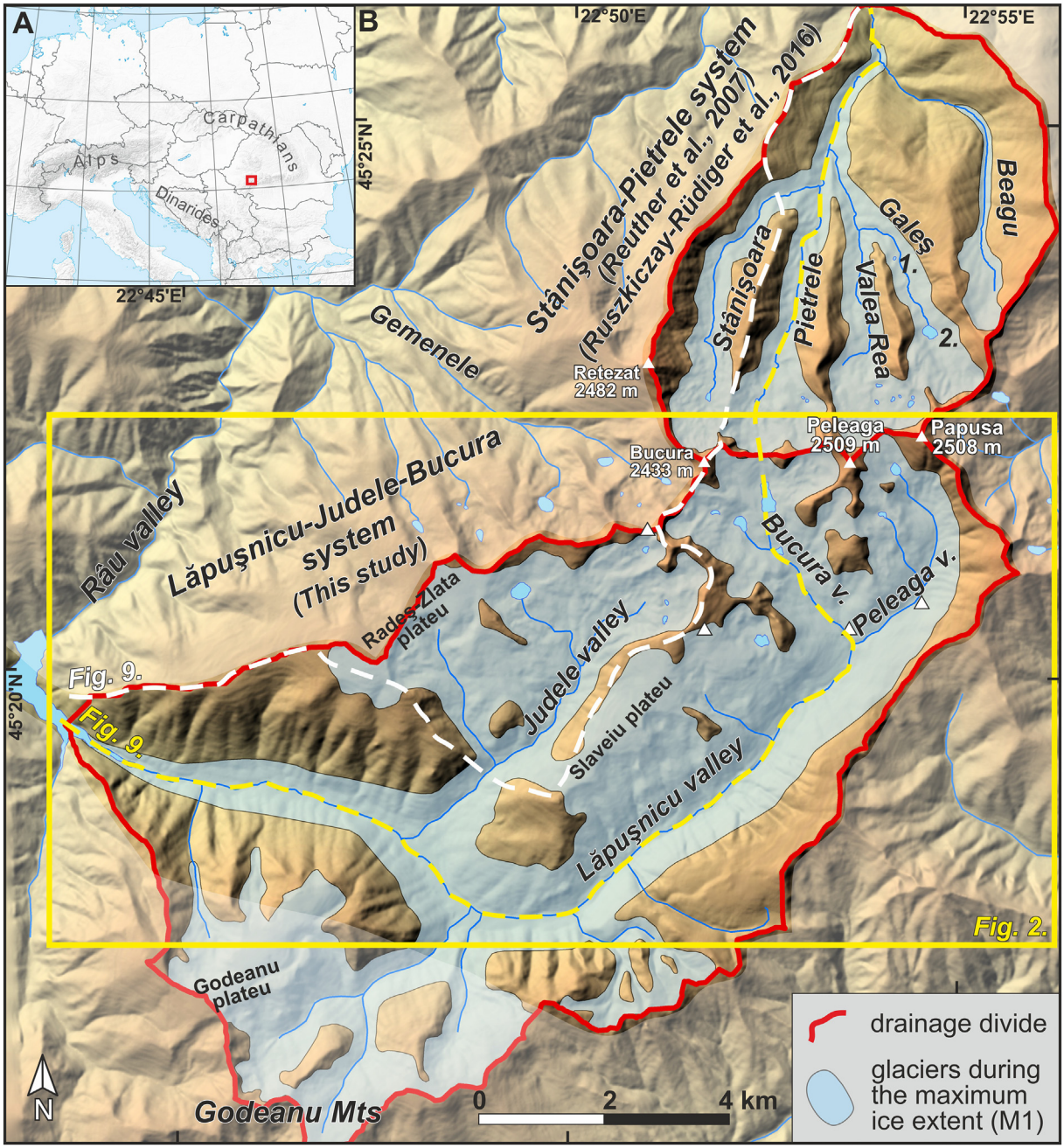

Fig. 1. A: Location of the Retezat Mts in Europe (red rectangle). B: Digital elevation model of the western and central part of Retezat Mts with the studied valley systems highlighted by red contours. The yellow rectangle is the study area as shown in Fig. 2. The dashed lines are the topographic profiles shown in Fig. 9 (white: ridge, yellow: valley). The glacier extent during the LGM (M1) is after Ruszkiczay-Rüdiger et al. (2018). 1. Lake Brazi, 2. Lake Galeş.

were interpreted as a sequence of moraines formed during the final deglaciation of the range, with the oldest moraine at the distal edge and the youngest one on the up-valley side of the system.

2.3. The hitherto published glacial chronology of the region and the study area

Since the beginning of the 21st century an increasing number of studies have been dedicated to the numerical age determination of the glaciations in the Western Carpathians, above all the Tatra Mts. (Engel et al., 2015, 2017; Makos et al., 2013a, 2013b, 2014, 2016, 2018; Zasadni and Kłapyta, 2016; Zasadni et al., 2020). Much less work has focussed on the age determination of glacial landforms in the Eastern (Gheorghiu, 2012; Rinterknecht et al., 2012) and Southern Carpathians (Reuther et al., 2007; Kuhlemann et al., 2013; Gheorghiu et al., 2015; Ruszkiczay-Rüdiger et al., 2016).

The data show a wide scatter concerning the timing of the final deglaciation: at some areas glaciers had already melted before the GS-1 or Younger Dryas (YD, 12.9–11.7 ka; Rasmussen et al., 2006), while at other locations they disappeared during or even after the YD (Makos et al., 2013b, 2018). The position of the moraines of the Last Glacial Maximum (LGM) phase is also under debate both throughout the Eastern (Gheorghiu, 2012; Kłapyta et al., 2020) and Southern Carpathians (Reuther et al., 2007; Ruszkiczay-Rüdiger et al., 2016). Here the term LGM is used in its broader sense (26–18 ka; Shakun and Carlson, 2010; Hughes et al., 2013) and the Lateglacial is considered as the period between the LGM and the Holocene (18–11.7 ka).

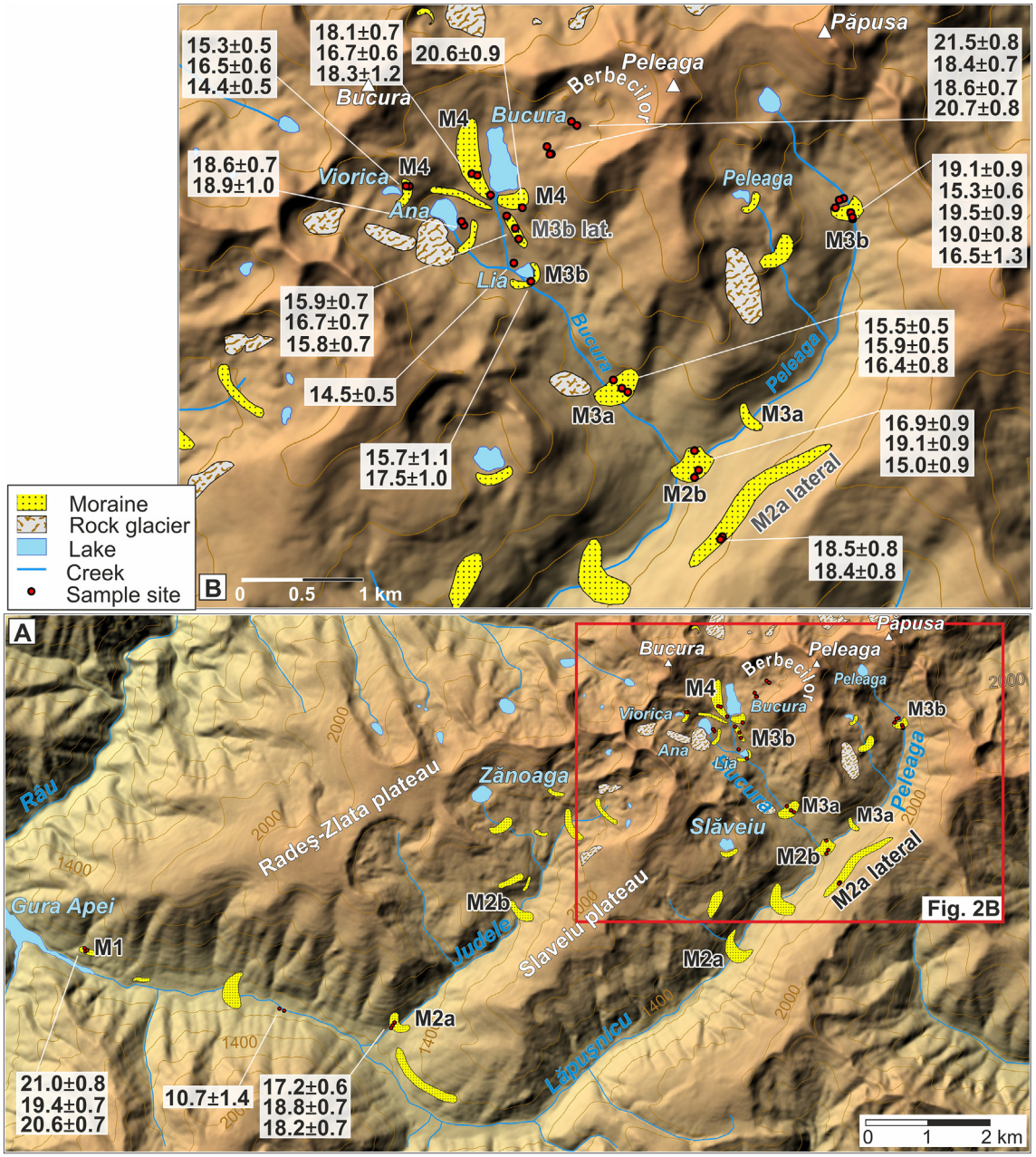

Fig. 2. Digital elevation model (DEM) and glacial landforms of the study area (modified after Urdea, 2000) with sample locations and CRE ages. M1-M4 indicates the position of the terminal moraines of the glacial phases discussed in this work (lateral moraines are indicated where sampled). Numbers are the CRE ages (ka) obtained by this study. A: The entire study area. Coordinates of the DEM: 45.37221N, 22.72200E (top left) and 45.29382N, 22.93783E (bottom right). For location refer to Fig. 1. B: Enlargement of the upper reach of the Bucura and Peleaga valleys. For sample codes see Table 2 and Fig. S1. In addition, the sample locations in KMZ format are added to the supplementary material.

In the Retezat Mts previous chronological works were restricted to the northern, Pietrele–Stânișoara valley system and no numerical ages of glacial landforms were available from valleys descending in other directions (Reuther et al., 2007, Ruszkiczay-Rüdiger et al., 2016). The first ^{10}Be CRE dating work (Reuther et al., 2007) combined with pedological investigations tentatively placed the MIE in the alpine early Würm (MIS 4) or an older phase (Riss, MIS 10-6) (Reuther et al., 2007; Urdea and Reuther, 2009). More recently, a recalculation of these ^{10}Be exposure ages in combination with new data suggested that the local MIE corresponded to the LGM (M1: $20.8^{+0.8}/_{-1.4}$ ka; Ruszkiczay-Rüdiger et al., 2016, the ages were recalculated using the same correction factors of this study, see Section 3.3 and Table S2). The deglaciation of the northern side occurred during the Lateglacial with four subsequent phases (M2a: $18.7^{+0.8}/_{-0.9}$ ka; M2b: $17.0^{+0.7}/_{-0.6}$ ka; M3: $15.5^{+0.8}/_{-0.8}$ ka and M4:$14.9^{+0.6}/_{-0.6}$ ka).

3. Materials and methods

3.1. Geomorphological mapping, fieldwork and sample collection

During the pre-fieldwork desk-mapping, the hand-drawn geomorphological map of the Retezat Mts (Urdea, 2000) was georeferenced and the glacial landforms were digitized in an ArcGIS environment. Next, the glacial landforms (lateral and terminal moraines, trimlines, glacially polished surfaces, plateus) were adjusted using a 10 m horizontal resolution digital elevation model (DEM), assisted by 3D imagery

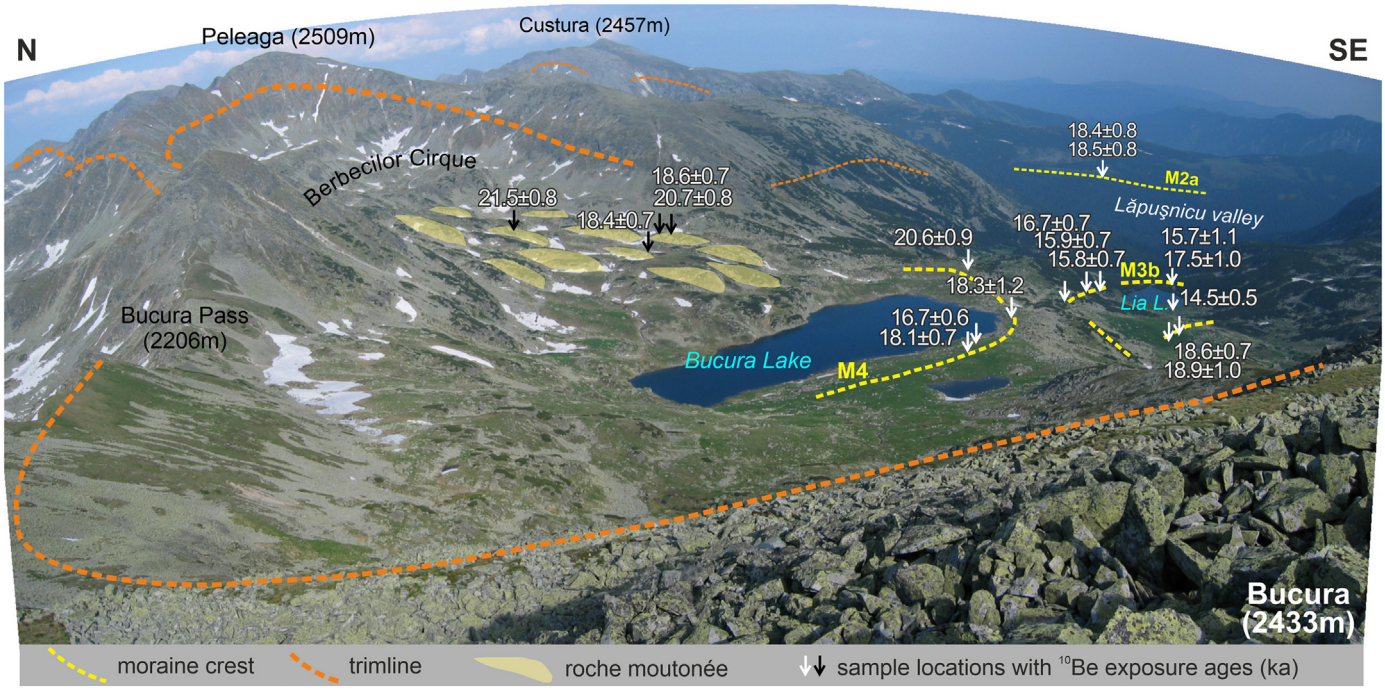

Fig. 3. Main ridge of the Retezat Mts, the Lake Bucura and the Berbecilor Cirque with the glacial landforms and the CRE ages (ka). The photo was taken from the Bucura peak, for location of the photo refer to Fig. 2.

provided by GoogleEarth. In the course of the fieldwork itself, the glacial geomorphological maps were refined and the targeted glacial landforms were selected (Fig. 2). The Lăpuşnicu–Bucura valley system is much longer and more gently sloping than the northern valleys, which enabled us to refine the previously established morpho-stratigraphic framework describing four to five deglaciation phases from the northern valleys (Urdea, 2000, 2004; Reuther et al., 2007; Ruszkiczay-Rüdiger et al., 2016). As a result, six deglaciation phases were distinguished. Keeping the scheme of the original fourfold division, these phases were termed as M1, M2a, M2b, M3a, M3b and M4, from the oldest/most extensive towards the youngest/least extensive phase (Fig. 2).

The samples were collected in 2015 ($n = 29$, among which four (Re15-4, -5, -6, -28) were not processed, and thus are missing from Tables 1, 2 and S1) and in 2016 ($n = 16$). The targeted objects were mostly large moraine- or solitary glacial boulders and, at two locations, ice-moulded bedrock surfaces. One sample from each boulder or bedrock surface was taken and at least two, but preferably three or more samples were taken from each moraine to provide a solid basis for the age determination of the relevant deglaciation phase.

The boulders were selected based on the following criteria: size (as large as possible), stable position (close to the moraine crest and with a top surface as flat as possible), with no signs of erosion or chipping (Balco, 2011, 2020; Heyman et al., 2016) (Figs. 4, 5). The samples were collected using hammer and chisel by chopping 1–3 cm thick chips from the rock surface. The position of the samples was measured using a hand-held GPS (Garmin etrex 30) and the elevation values were derived from the DEM. The strike and dip of the samples were measured using a Suunto Tandem compass-clinometer (Tables 1, S1).

In the following the sampled locations are described in the context of their morpho-stratigraphic position, which served as a guideline for our sampling strategy.

During the MIE, large plateau glaciers occupied the high elevation (2100–2200 m asl) smooth Radeş-Zlata plateau to the northwest of the Judele valley and the smooth, flat topped Slăveiu ridge (2200–2000 m) between the Judele and Lăpuşnicu valleys. The valley glaciers were partially fed by these ice fields, as it has been also reconstructed in the case of the neighbouring Godeanu Mts (Ignéczi and Nagy, 2016) (Fig. 1). The highest peaks (>2300 m asl) rose above the ice field, separating the southern, northern and western glacier systems (Figs. 1, 2). The present-day drainage divide between the northern and southern valley systems likely coincides with the former ice-divide (Figs. 1, 3). The terminal moraine (M1) of the MIE was difficult to map in the Lăpuşnicu valley, due to the presence of the artificial Lake Gura Apei. Large boulders were grouped at an elevation of ~1130 m asl elevation on the lower slopes of the valley, and these may be interpreted as remnants of the latero-frontal moraine complex of the MIE (samples Re15-01, -02, -03, Fig. 4A, for sample codes in map view see Fig. S1). Besides, a huge erratic boulder was sampled on the valley floor of the Lăpuşnicu valley between the M1 and M2a moraines (Re15-29).

In the next, M2a glacial phase the glaciers coming from the Godeanu Mts and from the Judele valley were separated from the main, Lăpuşnicu glacier. The glacier descending from the Judele valley approached its confluence with the Lăpuşnicu valley, at an elevation of ~1280 m, where its frontal moraine was sampled (Re15-07, -08, -09; Fig. 4B). Three additional samples (Re15-04,-05,-06) were also collected close to this moraine, but these were not processed due to their less favourable morphological position. In the Lăpuşnicu valley the terminal moraines belonging to the M2a phase were mapped further up-valley, at ~1450 m asl (not sampled due to the lack of suitable boulders). The substantial loss of its feeding area could lead to the observed more considerable retreat of the main, Lăpuşnicu glacier, compared to the relatively smaller retreat of the Judele glacier. A lateral moraine of this phase was sampled ~200 m above the valley floor close to the confluence of the Bucura and Peleaga valleys (Re16-01, -02; Figs. 2, 3). The boulder of the Re16-02 sampled was lying on a sloping surface and was partly covered by soil. In the lack of other suitable boulders on the targeted moraine its uncovered part was sampled. It was interpreted as exhumed from under an up to ~30 cm thick soil cover. Therefore, a mean soil cover of 15 cm was estimated for the entire exposure duration of this sample and the calculated age was corrected using this value. If no soil cover was applied, the resulting CRE age would be 11% younger, and the application of a

Table 1
Sample data for cosmogenic ^{10}Be exposure age determination. Some boulders in the lower, forested area were covered by a thin organic-rich soil, whose density was estimated at 0.9 g/cm^3. These samples and the corresponding thickness of the soil cover are the following: Re15–01: 6 cm, Re15-02: 5 cm, Re15-03: 1 cm, Re15-07: 3 cm, Re15-08: 7.5 cm, Re15-09: 2 cm, Re15-23: 2 cm and Re16-02: 30 cm (more developed soil with a density of 1.2 g/cm^3). The rest of the samples were uncovered. M1: relevant glacial phase; fm: frontal moraine; lm: lateral moraine; bf: boulderfield; gb: glacial boulder; rm: roche moutonnée; Lap: Lăpuşnicu valley; Buc: Bucura valley; Pel: Peleaga valley; Jud: Judele valley; M.Buc: Bucura Moraine; M.Vio: Viorica Moraine; C. Ber: Berbecilor Cirque. For more sample data refer to Table S1.

Sample ID	Latitude	Longitude	Elevation	Thickness	Boulder size (m)			Valley	Morphostrat
	(N,°)	(E,°)	(m, asl)	(cm)	Length	Width	Height		
Re15-01	45.32296	22.73947	1134	1.0	6.5	4.0	5.0	Lap	M1, fm
Re15-02	45.32246	22.73967	1125	0.9	3.0	2.0	1.5	Lap	M1, fm
Re15-03	45.32265	22.74004	1133	1.0	3.6	1.3	0.8	Lap	M1, fm
Re15-07	45.31234	22.80453	1295	0.9	4.0	2.2	1.6	Jud	M2a, fm
Re15-08	45.31189	22.80410	1281	2.0	3.5	4.5	3.5	Jud	M2a, fm
Re15-09	45.31153	22.80382	1274	2.5	4.8	2.9	2.8	Jud	M2a, fm
Re15-10	45.35852	22.86547	2088	1.0	1.7	1.6	1.3	M.Vio	M4, fm
Re15-11	45.35852	22.86547	2088	1.0	2.6	1.5	1.3	M.Vio	M4, fm
Re15-12	45.35854	22.86512	2087	1.0	1.7	1.5	1.2	M.Vio	M4, fm
Re15-13	45.35946	22.87180	2072	1.5	2.0	2.5	0.8	M.Buc	M4, fm
Re15-14	45.35934	22.87236	2070	1.5	4.8	3.8	0.9	M.Buc	M4, fm
Re15-15	45.35794	22.8737	2047	0.9	3.7	2.7	2.1	M.Buc	M4, fm
Re15-16	45.35705	22.87696	2051	2.0	2.1	2.1	1.2	M.Buc	M4, fm
Re15-17	45.35646	22.87538	1998	2.5	2.8	2.1	1.1	Buc	M3b, lm
Re15-18	45.35556	22.87626	1985	1.0	4.9	4.1	3.5	Buc	M3b, lm
Re15-19	45.35481	22.87662	1960	1.5	4.2	2.2	1.8	Buc	M3b, lm
Re15-20	45.35176	22.87788	1912	2.5	4.0	3.3	2.9	Buc	M3b, fm
Re15-21	45.35176	22.87788	1912	1.5	3.3	2.4	2.3	Buc	M3b, fm
Re15-22	45.35307	22.87612	1914	0.9	10.0	5.0	2.6	Buc	>M3b, gb
Re15-23	45.34473	22.88634	1745	1.0	2.7	1.9	1.6	Buc	M3a, fm
Re15-24	45.34414	22.88720	1730	1.0	3.6	3.2	1.9	Buc	M3a, fm
Re15-25	45.34387	22.88781	1727	1.5	4.1	3.4	2.0	Buc	M3a, fm
Re15-26	45.33970	22.89464	1629	3.0	5.8	4.4	2.6	Lap	M2b, bf
Re15-27	45.33831	22.89507	1625	1.0	6.0	5.5	3.2	Lap	M2b, bf
Re15-29	45.31425	22.78038	1167	1.0	15.0	5.0	5.0	Lap	>M1; gb
Re16-01	45.33355	22.89755	1773	2.0	4.0	5.5	0.9	Lap	M2a, lm
Re16-02	45.33334	22.89734	1774	1.0	2.7	2.4	0.7	Lap	M2a, lm
Re16-03	45.35686	22.91037	1869	1.5	6.0	4.5	4.2	Pel	M3b, fm
Re16-04	45.35641	22.91056	1870	1.5	3.3	2.7	1.6	Pel	M3b, fm
Re16-05	45.35652	22.91052	1874	1.5	2.6	2.2	1.5	Pel	M3b, fm
Re16-06	45.35788	22.90961	1876	1.0	5.0	3.3	1.4	Pel	M3b, fm
Re16-07	45.35776	22.90919	1892	0.8	3.3	1.7	3.8	Pel	M3b, fm
Re16-08	45.35721	22.90879	1904	2.0	2.4	1.7	1.0	Pel	M3b, lm
Re16-09	45.36327	22.88187	2161	2.0	–	–	1.0	C.Ber	>M4; rm
Re16-10	45.36297	22.88244	2141	2.0	3.8	2.7	1.6	C.Ber	>M4; gb
Re16-11	45.36144	22.87944	2117	2.0	4.1	4.5	3.1	C.Ber	>M4; gb
Re16-12	45.36092	22.87987	2128	1.5	6.0	2.7	2.4	C.Ber	>M4; gb
Re16-13	45.36090	22.87974	2129	2.0	–	–	1.0	C.Ber	>M4; rm
Re16-14	45.35576	22.87102	1977	0.8	4.9	3.4	2.1	C.Buc	>M3b; gb
Re16-15	45.35603	22.87077	1983	2.0	3.8	3.5	1.2	C.Buc	>M3b; gb
Re16-16	45.33778	22.89467	1614	1.8	4.2	3.6	2.6	Lap	M2b, bf

double thickness of soil cover would make the CRE age 12% older. Keeping the soil cover within 10 cm and 20 cm, as estimated in the field, leads to a variability of 4% of the CRE age, which is within the uncertainty of the method.

The boulderfield in the junction of the Bucura and Peleaga valleys consists of several large boulders scattered on a wide and relatively flat area at ~1620 m asl. According to the geomorphological mapping, the position of these boulders may correspond to a moraine representing the glacier termination during the M2b phase (Figs. 2, 4C), however the moraine itself has most probably been reworked by fluvioglacial and paraglacial processes. Three samples were taken from this landform (Re15-26, -27, Re16-16), hoping that their size prevented them to be considerably disturbed by these post-depositional processes.

After this phase the receding Lăpuşnicu glacier was split up to its two main tributaries occupying the Bucura and Peleaga valleys. In the Bucura valley, the terminal moraine of the M3a glacier was reconstructed at ~1710 m (Re15-23, -24,-25; Fig. 4D). In the Pelega valley it was less expressed at ~1680 m, and it could not be sampled in the lack of suitable boulders. The frontal moraine of the M3b phase is damming the Lake Lia (~1910 m; Re15-20, -21), and it has a well-defined left-lateral moraine (Re15-17, -18, -19, Figs. 2, 3, 4E, F). A sample was taken from a glacial boulder situated on the valley floor above Lake Lia (Re15-22). Higher in this valley, at ~1870 m asl, a latero-frontal moraine and some glacial boulders behind the moraine were mapped, considered to belong to the M3b phase (Re16-03, -04, -05, -06, 07, 08). Two glacial boulders were sampled next to Lake Ana, in a position between M3b and M4 moraines (Re16-14, -15).

The moraines of the cirque areas in front of Lakes Bucura and Viorica were considered to belong to the youngest deglaciation phase (M4) with terminal moraines at ~2050–2090 m asl. Samples were collected in two cirques of the Bucura valley: in front of Lake Viorica (Re15-10, -11, -12) and in front of Lake Bucura (Re15-13, -14, -15, -16). The large, shallow Berbecilor Cirque above Lake Bucura is characterised by a glacially sculpted landscape with frequent occurrence of glacially moulded roches moutonnées and whalebacks of 10 to 20 m height. Most of these landforms are uncovered except for scattered glacial boulders deposited on their top and in between (Figs. 3, 8). In order to test whether glacial erosion was deep enough in the cirque area to remove all CRN inventories from preceding exposures, the stoss-and-lee landforms were sampled at two locations (Re16-09; Re16-13) and boulders were sampled next to the glacial knobs (Re16-10, -11) and on top of them (Re16-12).

Table 2
Measured ^{10}Be concentrations and calculated surface exposure durations. The measured ^{10}Be/^{9}Be AMS ratios were corrected for full processed blank ratios: $(4.07 \pm 0.49) \times 10^{-15}$ for samples Re15-01 to -14; $(3.30 \pm 0.50) \times 10^{-15}$ for samples Re15-15 to -29; $(3.13 \pm 0.60) \times 10^{-15}$ for samples Re16-01 to -07; $(3.43 \pm 1.12) \times 10^{-15}$ for samples Re16-08 to -14 and $(3.67 \pm 0.83) \times 10^{-15}$ for samples Re16-15 to -16. Age uncertainties: the 1st number is the internal uncertainty (AMS measurement, weighting, carrier, blank and half-life; 1σ) and the 2nd number (external uncertainty, in parenthesis) includes the uncertainty of the reference production rate as well. *Every reported age was corrected for topographic- and self-shielding. **Corrected also for surface denudation (2 mm/kyr), uplift (1 mm/yr) and snow and soil shielding. For correction factors used for the age calculation, refer to Table S1. The exposure durations calculated using all corrections are acceptd and discussed by this study (printed in bold).

Sample ID	Blank corrected ^{10}Be concentration (at/gr$_{SiO2}$)	Exposure duration*(ka)	Exposure duration*(ka)
		No correction	All corrections**
Re15-01	195,329 ± 7588	19.6 ± 0.8 (1.8)	**21.1 ± 0.8 (1.9)**
Re15-02	180,515 ± 6130	18.2 ± 0.6 (1.6)	**19.4 ± 0.7 (1.7)**
Re15-03	191,915 ± 6506	19.3 ± 0.7 (1.7)	**20.6 ± 0.7 (1.8)**
Re15-07	179,259 ± 6023	16.2 ± 0.6 (1.4)	**17.2 ± 0.6 (1.5)**
Re15-08	186,479 ± 6478	17.4 ± 0.6 (1.6)	**18.8 ± 0.7 (1.7)**
Re15-09	180,421 ± 6379	17.1 ± 0.6 (1.5)	**18.2 ± 0.7 (1.6)**
Re15-10	271,848 ± 9373	13.2 ± 0.5 (1.2)	**15.3 ± 0.5 (1.4)**
Re15-11	292,942 ± 10,485	14.2 ± 0.5 (1.3)	**16.5 ± 0.6 (1.5)**
Re15-12	255,357 ± 8532	12.4 ± 0.4 (1.1)	**14.4 ± 0.5 (1.3)**
Re15-13	317,827 ± 11,228	15.5 ± 0.6 (1.4)	**18.1 ± 0.7 (1.6)**
Re15-14	288,153 ± 9754	14.3 ± 0.5 (1.3)	**16.7 ± 0.6 (1.5)**
Re15-15	324,684 ± 21,047	16.1 ± 1.1 (1.7)	**18.3 ± 1.2 (1.9)**
Re15-16	354,329 ± 14,557	17.7 ± 0.7 (1.6)	**20.6 ± 0.9 (1.9)**
Re15-17	263,086 ± 12,368	13.7 ± 0.7 (1.3)	**15.9 ± 0.7 (1.5)**
Re15-18	290,511 ± 12,139	15.0 ± 0.6 (1.4)	**16.7 ± 0.7 (1.5)**
Re15-19	263,012 ± 10,816	14.0 ± 0.6 (1.3)	**15.8 ± 0.7 (1.5)**
Re15-20	255,046 ± 18,621	14.2 ± 1.0 (1.6)	**15.7 ± 1.2 (1.7)**
Re15-21	285,192 ± 16,032	15.8 ± 0.9 (1.6)	**17.5 ± 1.0 (1.8)**
Re15-22	239,699 ± 7960	13.1 ± 0.4 (1.1)	**14.5 ± 0.5 (1.3)**
Re15-23	216,726 ± 7318	14.0 ± 0.5 (1.2)	**15.5 ± 0.5 (1.4)**
Re15-24	229,067 ± 7639	14.7 ± 0.5 (1.3)	**15.9 ± 0.5 (1.4)**
Re15-25	233,970 ± 11,418	15.2 ± 0.8 (1.5)	**16.4 ± 0.8 (1.6)**
Re15-26	229,290 ± 12,093	15.8 ± 0.8 (1.6)	**16.9 ± 0.9 (1.7)**
Re15-27	260,797 ± 12,640	17.8 ± 0.9 (1.7)	**19.1 ± 0.9 (1.8)**
Re15-29	103,086 ± 13,394	10.3 ± 1.3 (1.6)	**10.7 ± 1.4 (1.7)**
Re16-01	276,136 ± 11,005	16.8 ± 0.7 (1.5)	**18.5 ± 0.7 (1.7)**
Re16-02	246,651 ± 9865	14.9 ± 0.6 (1.4)	**18.4 ± 0.8 (1.7)**
Re16-03	296,997 ± 13,388	17.3 ± 0.8 (1.6)	**19.1 ± 0.9 (1.8)**
Re16-04	230,750 ± 9035	13.7 ± 0.5 (1.2)	**15.3 ± 0.6 (1.4)**
Re16-05	No current	No current	**No current**
Re16-06	291,447 ± 12,902	16.9 ± 0.8 (1.6)	**19.5 ± 0.9 (1.8)**
Re16-07	297,129 ± 11,848	17.2 ± 0.7 (1.6)	**19.0 ± 0.8 (1.7)**
Re16-08	252,034 ± 20,434	14.4 ± 1.2 (1.7)	**16.5 ± 1.3 (1.9)**
Re16-09	389,814 ± 14,971	18.3 ± 0.7 (1.7)	**21.5 ± 0.8 (2.0)**
Re16-10	No current	No current	**No current**
Re16-11	343,696 ± 13,123	16.5 ± 0.6 (1.5)	**18.4 ± 0.7 (1.7)**
Re16-12	349,112 ± 13,687	16.7 ± 0.7 (1.5)	**18.6 ± 0.7 (1.7)**
Re16-13	367,412 ± 14,022	17.6 ± 0.7 (1.6)	**20.7 ± 0.8 (1.9)**
Re16-14	313,159 ±1 2,005	16.3 ± 0.6 (1.5)	**18.6 ± 0.7 (1.7)**
Re16-15	308,130 ± 16,588	16.3 ± 0.9 (1.6)	**18.9 ± 1.0 (1.9)**
Re16-16	203,806 ± 12,102	14.1 ± 0.8 (1.4)	**15.0 ± 0.9 (1.5)**

3.2. Sample treatment and measurement

Sample processing was performed at the Cosmogenic Nuclide Sample Preparation Laboratory of the Institute for Geological and Geochemical Research (Budapest, Hungary). Samples were crushed and sieved to a grain size of 0.25–1 mm. The quartz content of the samples was enriched via density separation using heavy liquids (LST Fastfloat). Chemical sample processing followed the procedures of Merchel and Herpers (1999) and Merchel et al. (2019): Each sample (~100 g) was chemically etched using a 1:1 mixture of HCl and H_2SiF_6, then the atmospheric ^{10}Be inventory was removed by the stochiometric dissolution of the outer 1/3 part of the quartz grains. The quality of the purified quartz was checked optically using a stereomicroscope and, if necessary, XRD (Rigaku Miniflex). 20–30 g of pure quartz was dissolved in HF (48%) in the presence of 300 μg ^{9}Be carrier (0.980 mg/g ^{9}Be Scharlab Be standard solution BE0350100). After having substituted HF with HCl, ion exchange columns (Dowex 1 × 8 and 50Wx8) were used to extract ^{10}Be. Purified BeO was mixed with Nb powder and targets were prepared for AMS (Accelerator Mass Spectrometry) measurement of their ^{10}Be/^{9}Be ratios at ASTER, the French national AMS facility located at CEREGE, Aix en Provence (Arnold et al., 2010). The Beryllium measurements were calibrated against the ASTER in-house STD-11 standard (^{10}Be/^{9}Be = (1.191 ± 0.013) × 10^{-11}, equivalent to NIST_27900 (Braucher et al., 2015), considering the ^{10}Be half-life of (1.387 ± 0.012) × 10^{6} years (Chmeleff et al., 2010; Korschinek et al., 2010). Analytical uncertainties (reported as 1σ) include uncertainties concerning sample weighing, AMS counting statistics, ^{10}Be/^{9}Be ratios of the standards and chemical blank measurements and an external AMS error of 0.5% (Arnold et al., 2010).

3.3. Calculation of the ^{10}Be CRE ages

In the lithosphere, terrestrial in situ-produced cosmogenic ^{10}Be is mainly produced from O and Si within quartz mineral lattice at or close to the surface. Interactions with three main types of secondary particles, high-energy neutrons, slow and fast muons, induce in situ-production of cosmogenic nuclides (Lal, 1991). Assuming that the production and denudation rates remained constant through time, the

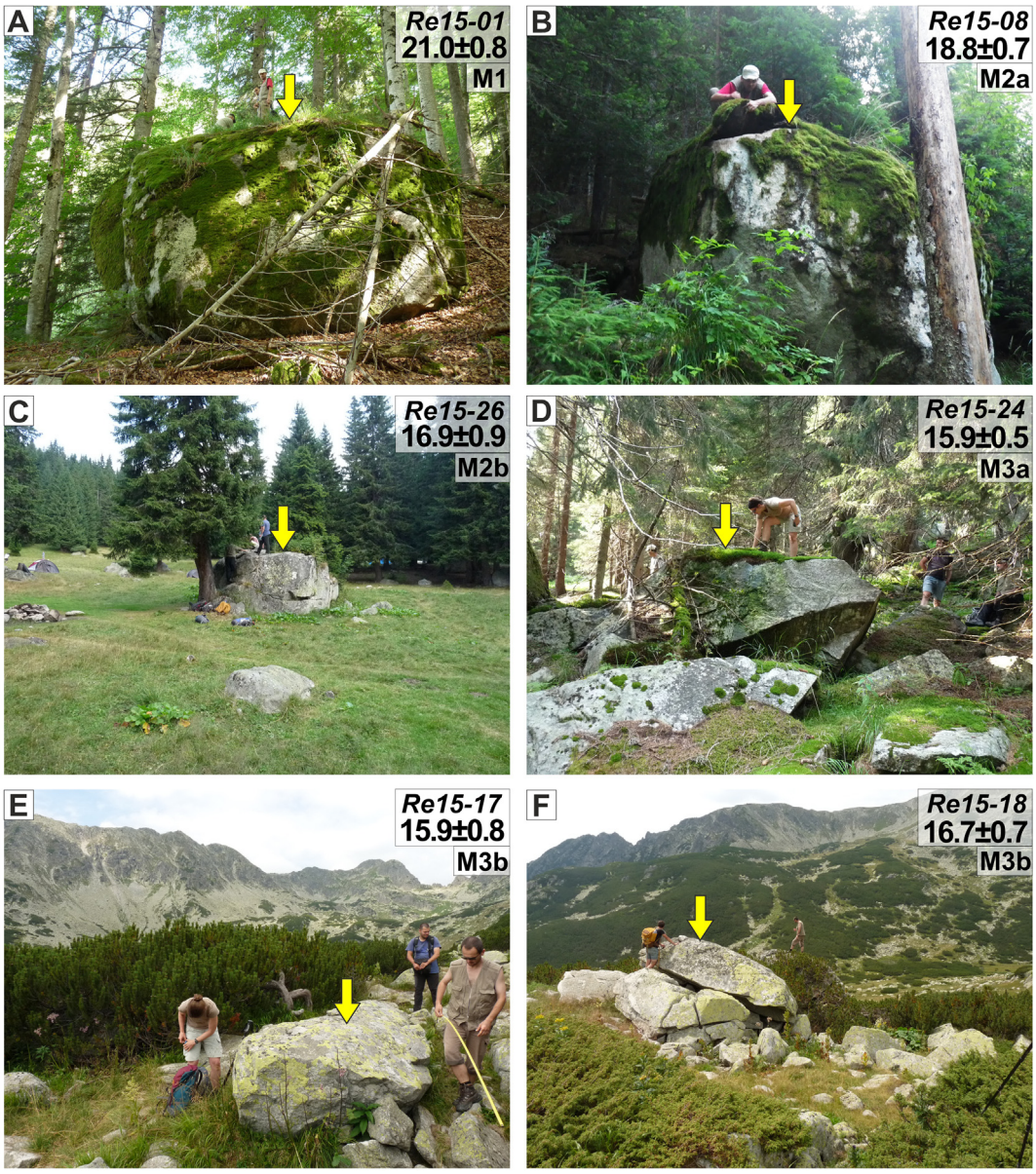

Fig. 4. Photos of sampled boulders (indicated by yellow arrows) with their sample code, CRE age (ka) and glacial phase in the top right corner. For locations refer to Table 1 and Figs. 2 and S1 and the supplementary kmz file.

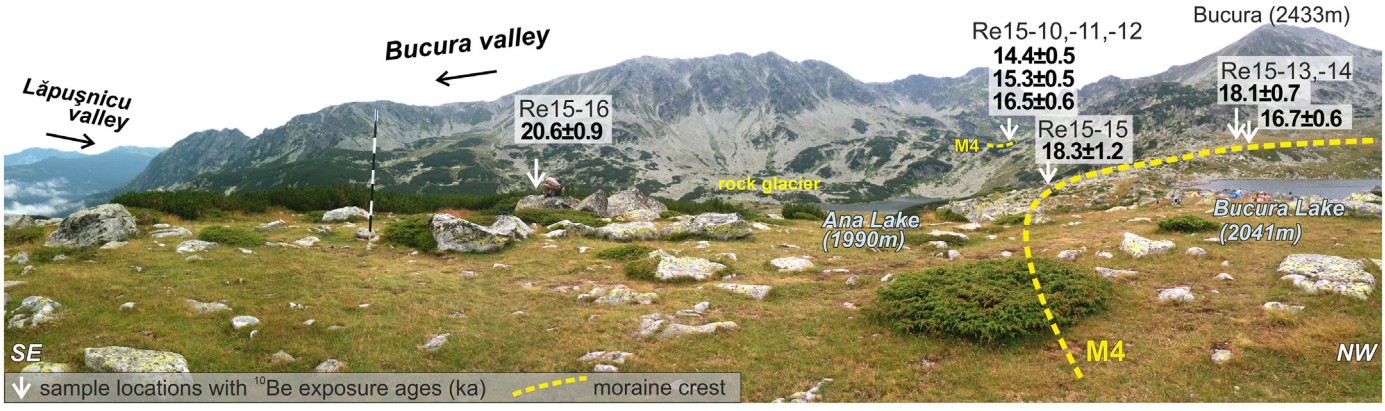

Fig. 5. Panoramic view of the Bucura moraine with the sampled boulders and their apparent CRE ages (ka). The photo was taken from the eastern termination of the M4 terminal moraine at Lake Bucura. For location see Fig. 2.

change of ^{10}Be concentrations over exposure time can be calculated using Eq. (1) (Braucher et al., 2003):

$$N_{(x,\varepsilon,t)} = \frac{P_{sp}.\exp\left(-\frac{x}{L_n}\right)\left(1-\exp\left(-t\left(\frac{\varepsilon}{L_n}+\lambda\right)\right)\right)}{\frac{\varepsilon}{L_n}+\lambda} + \frac{P_{\mu slow}.\exp\left(-\frac{x}{L_{\mu slow}}\right)\left(1-\exp\left(-t\left(\frac{\varepsilon}{L_{\mu slow}}+\lambda\right)\right)\right)}{\frac{\varepsilon}{L_{\mu slow}}+\lambda} + \frac{P_{\mu fast}.\exp\left(-\frac{x}{L_{\mu fast}}\right)\left(1-\exp\left(-t\left(\frac{\varepsilon}{L_{\mu fast}}+\lambda\right)\right)\right)}{\frac{\varepsilon}{L_{\mu fast}}+\lambda} + N_{inh}.\exp\left(-\lambda.t\right) \quad (1)$$

where N(x,ε,t) is the nuclide concentration in function of depth x [g/cm^2], denudation rate ε [g/cm^2/y] and exposure time t [y]. P_{sp}, $P_{\mu slow}$, $P_{\mu fast}$ and L_n, $L_{\mu slow}$, $L_{\mu fast}$ are the production rates and attenuation lengths of neutrons, slow muons and fast muons, respectively. Site specific production rates of in situ produced cosmogenic ^{10}Be were calculated using the CosmoCalc 3.0 Excel add-in (Vermeesch, 2007) employing the time-independent Lal (1991)/Stone (2000) scaling and a sea level high latitude (SLHL) spallogenic ^{10}Be production rate (P_{SLHL}) of 4.01 ± 0.33 at/g/yr (Borchers et al., 2016). $P_{\mu slow}$, $P_{\mu fast}$ are based on Braucher et al. (2011). The L_n, $L_{\mu slow}$, $L_{\mu fast}$ values used in this paper are 160, 1500 and 4320 g/cm^2, respectively (Gosse and Phillips, 2001; Heisinger et al., 2002a, 2002b). λ is the radioactive decay constant of ^{10}Be: (4.9975 ± 0.0432) × 10^{-7} y^{-1}. N_{inh} is the inherited nuclide concentration [at/g]. The internal uncertainties of the reported ages comprise the analytical uncertainties and the uncertainty of the half-life of ^{10}Be. External uncertainties include the uncertainty of the ^{10}Be production rate (Table 2).

Site-specific production rates were corrected for topographic shielding, self-shielding, snow-shielding (S_{Sw}) and soil-shielding (if relevant). Topographic shielding was calculated using the 10 m resolution DEM in ArcGIS environment (Codilean, 2006; Li, 2013). The correction for self-shielding occurred using the exponential function of Lal (1991) assuming a rock density of 2.7 g/cm^3. Self-shielding, snow-shielding and soil-shielding (if relevant) were calculated as using equations given by Vermeesch (2007) as described by Ruszkiczay-Rüdiger et al. (2020).

Snow shielding, which is a considerable factor in the calculation of exposure durations (Hippe et al., 2014), was estimated from the mean annual snow depth and snow cover duration at each sample site (ρ_{sw} = 0.3 g/cm^3, Λ_n = 160 g/cm^3). Mean annual snow depth at the sampling locations was calculated from corresponding values extracted from the gridded (1 × 1 km) datasets of monthly mean snow depth of Romania (Dumitrescu et al., 2017). The mean annual snow pack duration is usually above 250 days in the Alpine region of the Romanian Carpathians (>2000 m asl; Micu, 2009) so this value was assigned to all sampling locations above 2000 m asl. The duration of the continuous snow cover correlates closely with altitude (Micu, 2009) with an empirically determined elevation gradient of 8 days/100 m, in the Southern Carpathians (Micu et al., 2015). Accordingly, the duration of mean annual snow cover at the elevation of the sampling points under 2000 m asl was estimated using this elevation gradient: starting from 250 days/year at 2000 m asl, and decreasing 8 days with every 100 m downwards. The mean annual snow cover was corrected for boulder height due to the fact that high boulders are covered by thinner snow layer and for shorter time compared to the ground level (Heyman et al., 2016). The correction was based on a field-based conservative estimate of the relationship between the decrease of snow cover with boulder height: in cases where the boulder was at least 60 cm higher than the average snow depth during the snow-covered season, the mean annual snow cover was reduced by 20%. If the height difference was more than 120 cm, the snow cover was reduced by 40%. The production rates were not corrected for vegetation cover.

The sampled boulders were mostly uncovered. In cases when a few cm thick layer of moss and a peat-like skeletal soil covered the boulder (like in Fig. 4A and B), the site specific production rates were corrected for the soil cover at a density of 0.9 g/cm^3. Assuming that during the first part of the exposure history of the boulder it was uncovered yet, the soil correction factor was calculated considering half of the measured soil depth (Tables 1, S1, S2). For the sample Re16-02, for which a former, more developed soil cover of ~30 cm was estimated (see Section 3.1) the correction for soil cover was calculated at a soil density of 1.2 g/cm^3.

The surface denudation rate of crystalline rocks in alpine environments is typically slow, 0.5–2.5 mm/kyr (Balco, 2011). In this study, a surface denudation rate of 2 mm/kyr is considered a conservative value, falling between the 3 mm/kyr suggested for granitic boulders (Ivy-Ochs et al., 2004) and the 0.2 mm/kyr suggested for homogeneous crystalline rocks (André, 2002) in a mid-latitude alpine environment.

According to thermochronologic and kinematic studies, the Cenozoic deformation pattern of the Southern Carpathians allows for a very limited amount of Quaternary uplift of the Retezat Mts (Maţenco, 2017). On the basis of geodetic data (Zugrăvescu et al., 1998) the recent, 1 mm/yr uplift rate was used during the CRE age calculations. CRE ages both with and without correction for snow- and soil-shielding, denudation and uplift are presented (Table 2), but only the corrected ones will be discussed in the following.

For the comparison of the new data with the formerly published data from the northern valleys of the Retezat Mts (Reuther et al., 2007; Ruszkiczay-Rüdiger et al., 2016), the latter were recalculated using the newly acquired, DEM-based topographic shielding and elevation values, self-, snow- and soil-shielding, local denudation rate, and uplift rate as described in this section (Table S2).

In order to reveal any systematic bias in the calculated exposure ages stemming from the application of the time independent Lal-Stone scaling, all CRE ages were calculated using the online calculators as well: the Cosmic ray Exposure Program (CREp; Martin et al., 2017), the Cronus-Earth online calculator version 3 (CronusV3; Balco et al., 2008) and the Cronus-Earth Web Calculator version 2.0 (CronusWeb; Marrero et al., 2016). For the age calculations both the time dependent Lal/Stone scaling Lm; (Balco et al., 2008) and the Lifton-Sato-Dunai scaling models (LSD and its nuclide dependent version LSDn; Lifton et al., 2014) were used. All calculators were set to use the most recent calibration dataset, the ERA-40 atmosphere model and the geomagnetic database of Lifton et al. (2014 for CronusWeb) and Lifton (2016) (for CronusV3 and CREp). The calculators were accessed in June 2020.

3.4. Selection of outliers and calculation of the most probable exposure ages of the deglaciation phases

For the calculation of the most probable CRE age of each deglaciation phase, samples belonging to the frontal and lateral moraines of each phase were considered. The glacial boulder (Re15-22, Re16-11, -12, -14, -15) and roche moutonnée samples (Re16-09, -13) are supposed to give an age post-dating the formation of the moraine above which they were released by the melting glacier. Accordingly, these were not considered during the calculation of the most probable age of the deglaciation phases.

As moraine stabilization must have been governed by regional climate change, the deglaciation is supposed to be synchronous in all valleys within a few kilometres distance of the study area. Even if local factors lead to some difference in the final stabilization, this is expected to remain under the uncertainty of the CRE dating method. Accordingly, in case of a moraine of a certain deglaciation phase was sampled at two locations, the CRE ages were treated together to derive the most probable age of moraine stabilization (relevant for the M2a, M3b and M4 phases).

For the estimation of the landform ages, samples with exposure durations overlapping within uncertainties were considered. Interestingly,

the moraines in the cirque area (M3b, M4), which are supposed to be representative of the last deglaciation phases, provided exposure durations with a large scatter between ~14 and ~21 ka (see Table 2 and Section 4.2). For age distributions of such a wide scatter statistical methods fail in the selection of the outliers (Balco, 2011), as data pairs or triplets would be statistically acceptable from the young middle or old part of the age distribution. However, relative chronological order of moraine generations is a priori constrained by their morphostratigraphical position implying that during the deglaciation process glacier still-stands and smaller re-advances leave a moraine succession with each landform being younger than its neighbour down-valley and the cirque glaciers being the last to disappear. Using this clue enabled us to reveal that the dataset for the uppermost landforms was strongly biased towards long exposure durations. This distribution suggests i) the CRE ages of these moraines scatter more than expected from measurement uncertainty only; ii) the main reason for the scatter may be the presence of variable amount of inherited ^{10}Be from prior exposure. Accordingly, for these landforms (M3b and M4) the approach of Applegate et al. (2012) was followed by accepting the youngest coherent group of samples (M3b) or the single youngest sample as the best estimate of the age (i.e. containing the least amount of inherited ^{10}Be) of the landform and the relevant phase of deglaciation.

Unfortunately, the widely scattered exposure durations of the three samples from the probably reworked boulderfield at the position of the M2b moraine could not be treated as a statistically coherent dataset either. Following the same line of arguments as before, the CRN age of the single sample that fulfilled the criterion to be younger than the adjacent moraine down-valley and older than the moraine up-valley was accepted as the best estimate of the age of the M2b deglaciation phase (Figs. 6, 7).

As a next step, probability density functions were fitted to each coherent CRE age group using the "Camelplot" MATLAB code (Balco, 2009). The ^{10}Be CRE ages of each deglaciation phase correspond to the most probable values of the studied probability density distributions and the associated uncertainties to the 68% confidence interval ($\pm 1\sigma$) (Fig. 7). In the following these will be discussed as most probable exposure ages.

3.5. Quantification of the amount of inherited ^{10}Be, thickness of rock eroded and tentative estimation of glacial erosion rates

In a sample set affected by inheritance the measured ^{10}Be concentration will be the lowest for the sample with no (or with the smallest) inheritance. The differences between the measured ^{10}Be concentration of the sample with no (or minimum) inheritance and all other samples will provide the best estimate on the amount of inherited cosmogenic ^{10}Be in these samples. Making use of the function describing the exponential decrease of the concentration of cosmogenic nuclides with depth (Eq. (1)), the inherited ^{10}Be inventory enables the calculation of the thickness of rock eroded during the last glacial phase. For these calculations the present day conditions were assumed for the estimation of the ^{10}Be production during the previous ice-free periods (correction factors, denudation rate, uplift as described in Section 3.3).

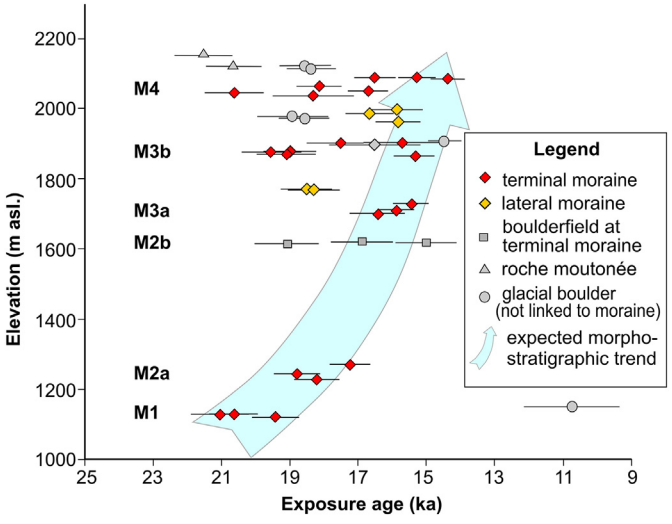

Fig. 6. Apparent CRE ages plotted against the elevations of the sample locations. Light blue arrow represents the expected morphostratigraphic trend of deglaciation-related terminal moraines being younger at higher position. Note that for the last two deglaciation phases (M3b and M4, above 1800 m asl) only the youngest samples follow this trend.

In this study, two models are presented showing the possible thickness of rock removed by the glacier. The first model is restricted to the last glacial-interglacial phase, while the second model extends back to the penultimate glacial cycle as well. The duration of glacier-covered and ice-free periods is estimated using speleothem U-Th ages gathered from several relict alpine caves in the Făgăraș Mts, to the east of the study area in the Southern Carpathians (Tîrlă et al., 2020). Speleothem growth in alpine karstic areas is a clear indicator of milder climate (i.e. warm and wet conditions and soil activity) while the lack of speleothem growth is typically interpreted as evidence of particularly dry and/or cold conditions (e.g. Spötl and Mangini, 2007; Ayalon et al., 2013; Stoll et al., 2013; Isola et al., 2019). This is because glacial conditions in the infiltration area of a cave would be a factor for reduced or ceased speleothem growth due to the depressed air temperatures (both at the surface and subsurface) strongly limiting water infiltration (Berstad et al., 2002) and totally inhibiting soil activity (McDermott, 2004).

In the alpine elevations of the Southern Carpathians speleothem formation occurred during warmer periods, largely corresponding to interglacial conditions. Hence, periods of speleothem growth in these relict caves situated in the cirque region (~2300 m asl) can be reliable indicators of ice-free conditions not only in the Făgăraș Mts but also in the surrounding massifs, such as the Retezat Mts. This dataset was used to find a suitable threshold separating the glacial and ice-free conditions in the study area in the benthic δ^{18}O record (Lisiecki and Raymo, 2005), which is a proxy for the global ice volume. Several threshold δ^{18}O values have been tested to find the most suitable threshold effectively separating glacial and interglacial conditions (Knudsen and Egholm, 2018). A δ^{18}O value of 4.25‰ was found suitable to separate periods with ice free conditions (i.e. speleothem growth) and likely glaciated conditions in the cirque region of the Southern Carpathians.

Additionally, once the thickness of material removed by the glacier and the duration of the glacial period are estimated, the time-averaged glacial denudation rate can also be assessed. However, during the interpretation of time-averaged glacial denudation rates it has always to be considered that glacial erosion is a discontinuous process, with glacial erosion possibly occurring only during restricted time intervals of the ice covered period. Taking into consideration that these long-term glacial denudation rates are not representative of the nature of subglacial erosion processes they are used merely for a comparison with results of studies providing similar data (Briner et al., 2006, 2016; Delmas et al., 2008; Crest et al., 2017; Valletta et al., 2017; Wirsig et al., 2017).

4. Results

4.1. The ^{10}Be concentrations and derived CRE ages

Altogether, 45 samples were taken, of which 41 were processed. Two of the processed samples had ^{10}Be/^{9}Be ratios under the detection limit of the AMS measurement (Tables 1, 2).

The ^{10}Be concentrations of the samples varied between $(389.8 \pm 15.0) \times 10^3$ at/g_{SiO2} and $(179.3 \pm 6.0) \times 10^3$ at/g_{SiO2} with a single value as low as $(103.1 \pm 13.4) \times 10^3$ at/g_{SiO2} considered as an outlier. The mean analytical uncertainty was 4.2%. The calculated CRE ages are between 21.5 ± 0.8 ka and 14.4 ± 0.5 ka, with a single sample (Re15-29) providing an apparent CRE age of 10.7 ± 1.4 ka (Table 2, Fig. 2).

The calculated ^{10}Be exposure ages show a normal morphostratigraphic trend, with decreasing ages up-valley from the moraines of the maximum

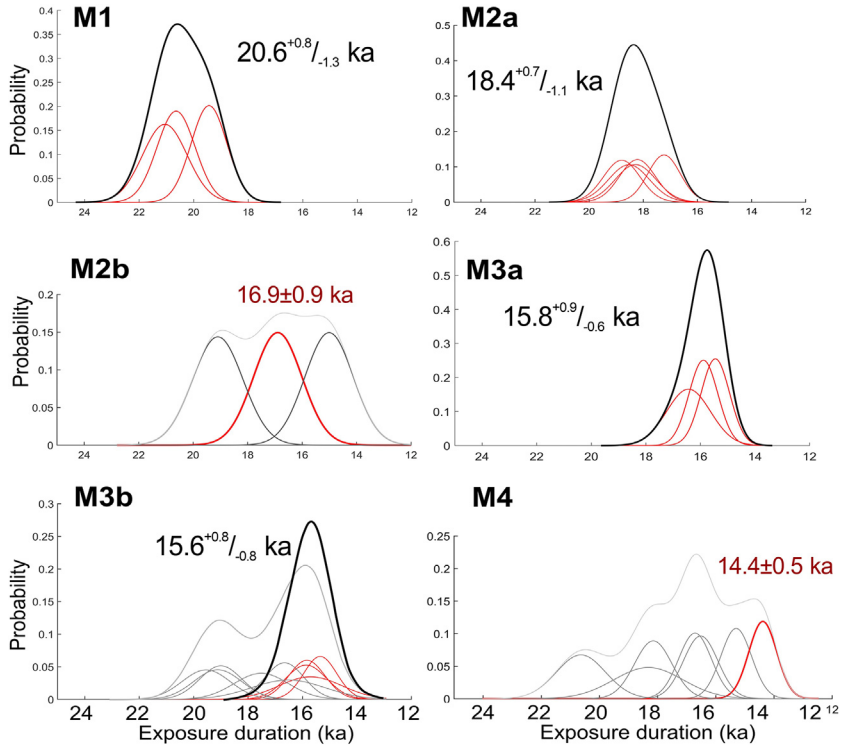

Fig. 7. Probability density distributions of the sample data and most probable ^{10}Be CRE durations of the glacier advances recognised in the Retezat Mts (thick black curves and numbers). For the M2b and M4 phases CRE age of a single sample could be accepted as the best estimate of the age of moraine abandonment by the glacier (red curves and numbers). Thin curves represent individual boulder CRE ages with the assumed Gaussian distribution of their uncertainty (red: accepted, grey: omitted as outlier).

ice extent (M1) up to ~1800 m asl, the elevation of the terminal moraines of the M3a phase (Fig. 6). The three samples from the M1 moraine provided a most probable CRE age of $20.6^{+0.8}/_{-1.3}$ ka. Unfortunately, the large boulder behind this moraine (Re15-29) provided an apparent exposure duration of 10.7 ± 1.4 ka most probably due to chipping or toppling of the boulder during the early Holocene. Based on five samples from terminal moraine in the Judele valley and the lateral moraine of the Lăpuşnicu valley, the most probable CRE age of the subsequent phase of deglaciation (M2a) was $18.4^{+0.7}/_{-1.1}$ ka (Figs. 6, 7, Table 2).

The wide scatter of the data coming from three samples from the boulderfield found at the position of the terminal moraine of the next (M2b) phase is problematic (Figs. 6, 7, Table 2). Among the three dated boulders, the CRE age of 16.9 ± 0.9 ka of sample Re16-26 is considered as best age estimate of this phase, fitting to the geochronological sequence of moraines, being always younger than the landform downvalley and older than the next moraine up-valley. The three samples taken from the frontal moraine of the subsequent deglaciation phase (M3a) provided a most probable CRE age of $15.8^{+0.9}/_{-0.6}$ ka (Figs. 6, 7).

The samples from the moraines of the M3b phase were taken from both the Bucura and Peleaga valleys ($n = 10$) and yielded apparent exposure durations distributed around two peaks (~19 ka and ~15.6 ka) (Fig. 7). The younger peak is in agreement with the morphostratigraphical position of the landform, suggesting that the remaining samples contain inherited ^{10}Be from prior exposure. Following the suggestion of Applegate et al. (2012) for moraines potentially affected by inheritance, the most probable CRE age of the younger coherent age group is accepted as the exposure age of the M3b stage at $15.6^{+0.8}/_{-0.8}$ ka (Re 15-17, -19, -20, Re16-04; Figs. 6, 7).

Seven samples were collected from the moraines of the last, M4 phase of deglaciation in two adjacent cirques of the Bucura valley (Fig. 2). The apparent CRE ages of these samples showed a wide scatter between 14.4 ± 0.5 ka (Re15-12) and 20.6 ± 0.9 ka (Re15-16), an age equivalent to the MIE or M1 (Figs. 2, 3, 7; Table 2). The morphostratigraphic position of this landform suggests that only the youngest apparent age is a relevant estimate of the time of moraine abandonment by the glacier (Fig. 6). The large number of apparent CRE ages much older than the most probable CRE age of the previous moraine (M3b), implies that the major part of the sampled M4 boulders carries a variable amount of cosmogenic ^{10}Be from prior exposure; therefore the CRE age of youngest sample (14.4 ± 0.5 ka; Re15-12) was accepted as the best estimate age of moraine stabilization for this phase.

The sampled glacial boulders and polished rock surfaces also provided considerably older ages than it was expected on the basis of their geomorphic position. Two boulders sampled between the M3b and M4 moraines next to Lake Ana provided 18.6 ± 0.7 ka and 18.9 ± 1.0 ka apparent exposure ages, which would correspond to the age of the second largest, M2a phase, when the glacier termination was ~13 km down-valley. Above the moraines of the M4 phase, the polished surface of the stoss-and-lee landforms from the Berbecilor Cirque yielded apparent exposure durations of 21.5 ± 0.8 ka (Re16-19) and 20.7 ± 0.8 ka (Re16-13), similar to the exposure age of the moraine generated during the LGM maximum ice extent (M1). The boulder samples from the same area provided exposure durations of 18.4 ± 0.8 ka (Re16-11) and 18.6 ± 0.7 ka (Re16-12), again resembling the age of the M2a phase (Fig. 8). The long apparent exposure durations of these samples at high altitude also provide a strong piece of evidence for the presence of excessive abundances of cosmogenic ^{10}Be in the cirque area due to an inherited CRN inventory (Figs. 6, 7, 8). The CRE age of a single boulder above the M3b moraine at Lake Ana (Re15-22; 14.5 ± 0.5) was younger than its morphostratigraphic position, most probably due to post-depositional chipping of its surface.

4.2. The CRE age estimates using time-dependent scaling schemes via online calculators

The CRE exposure durations using the same correction factors (described in Section 3.3) as applied during our calculations using Eq. (1) were also calculated by the online calculators, which enable the comparison of several scaling schemes in terms of the resulting CRE ages.

The time dependent Stone scaling (Lm) via the CREp (Martin et al., 2017) calculator provided 0.3–3.2% younger ages, the CronusV3 (Balco

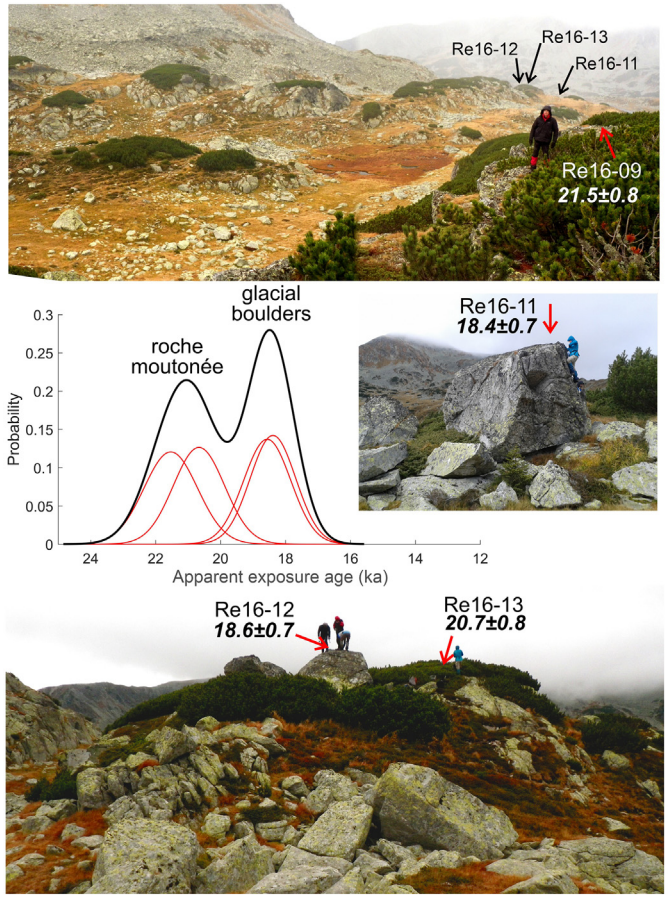

Fig. 8. Glacially sculpted landscape of the Berbecilor Cirque with roche moutonnée-s and glacial boulders. Sample locations are indicated. The probability density plots of their CRE ages show that apparent CRE durations of the bedrock and boulder samples (black numbers, ka) are similar to those of the MIE (M1) and M2a phases, respectively.

et al., 2008) resulted in 0.3% older to 4.1% younger ages and the CronusWeb (Marrero et al., 2016) provided 2.4% older to 0.8% younger ages compared to the values calculated using Eq. (1) and time independent Lal/Stone scaling (Table 2). When the LSDn scaling was applied the results varied between ±4.2% with the CREp, +3.6% to −6.7% using the CronusV3 and +5.4% to −2.8% using the CronusWeb calculator compared to the calculations using Eq. (1) with the Stone (2000) time independent scaling carried out in the present research.

Accordingly, exposure durations calculated by the time-dependent scaling models using the online calculators are within uncertainty, and thus indistinguishable from the values calculated in this study using the time-independent Lal/Stone scaling via Eq. (1). Besides, the calculated ages varied up to ~5% between calculators (due to using a slightly different set of equations and CRN production rate calibration datasets) and also displayed a degree of variability over a similar range depending on the atmosphere model and geomagnetic database used for the elevation-atmospheric pressure conversion and for the time-variant scaling, respectively. Therefore, in this study the exposure durations presented in Table 2, calculated using the time-independent Lal/Stone scaling via Eq. (1) are considered as reliable and will be discussed in the following.

5. Discussion

5.1. The deglaciation history of the study area

In this section the last deglaciation of the Retezat Mts be will be discussed using the most probable exposure durations of the mapped deglaciation phases derived from the new cosmogenic ^{10}Be data from the southern valleys and the recalculated data from the northern valleys (Figs. 2, 9; S1, Tables 2, S2).

The largest mapped ice extent (M1) was dated to $20.6^{+0.8}/_{-1.3}$ ka in the southern and to $20.8^{+0.8}/_{-1.3}$ ka in the northern valleys. During this phase the Lăpuşnicu Glacier was also fed by the Judele Glacier and by glaciers to the south of the Retezat Mts, descending from the Godeanu Ice Field (Ignéczi and Nagy, 2016). No glacial landforms and sediments could be mapped in lower, more distal positions (Figs. 1, 2). If there were previous, more extended glaciations, their signs have been destroyed by erosion. The MIE coinciding with the LGM (MIS 2) is in line with several published glacial chronologies from the continental areas of Central, Eastern, and Southern Europe.

In the Western Carpathians the LGM typically appears to be the most extended phase (Engel et al., 2015, 2017), although occasionally the existence of a previous, more extensive glacial advance has been confirmed (Makos et al., 2018). In the central Balkan Peninsula, the MIE moraines were attributed to the LGM (Kuhlemann et al., 2009, 2013, Ruszkiczay-Rüdiger et al., 2020), as was also the case of mountain ranges in Western Central Europe (Mentlik et al., 2013; Engel et al., 2014). In the Alps the glaciers reached their largest LGM position between ~26 and ~23 ka (Ivy-Ochs, 2015; Wirsig et al., 2016), slightly earlier than the M1 in the Retezat Mts. However, previous Alpine glaciations (MIS 6 or older) have been described as more extensive (Van Husen, 2004; Graf et al., 2015; Salcher et al., 2015). Similarly, the terminal moraines of the MIE were considered to have been produced by pre-LGM glaciations along the Adriatic Coastal Ranges (Hughes et al., 2010, 2011), although LGM ages were also reported (Çiner et al., 2019; Sarıkaya et al., 2020).

The considerable shortening of the Lăpuşnicu Glacier between M1 and M2a must have been the result of the separation of the glaciers draining from the Godeanu Ice Field and by the Judele glacier from the main, Lăpuşnicu Glacier. The age of this stage is $18.4^{+0.7}/_{-1.1}$ ka and

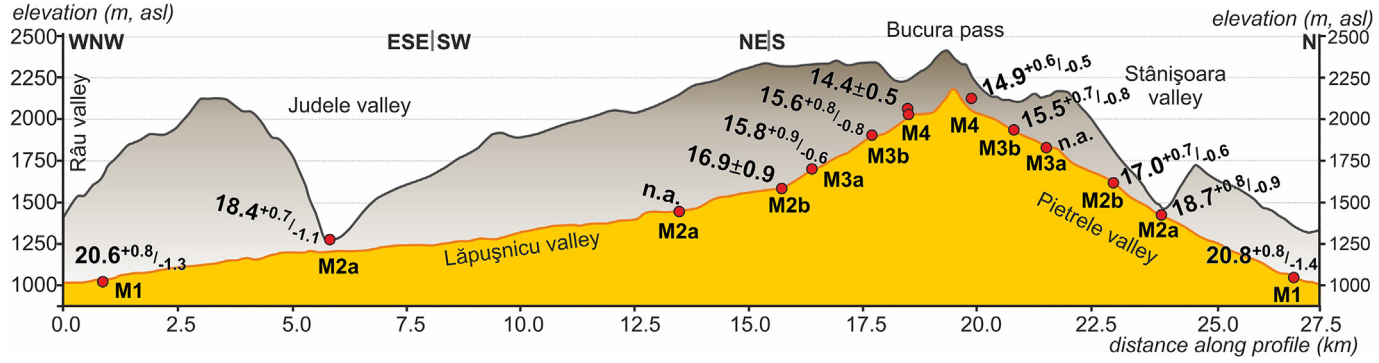

Fig. 9. South-north transect along the Lăpuşnicu and Bucura valleys to the Piertele valley (for location refer to Fig. 1B). The position of the terminal moraines and most probable CRE durations (ka) of the relevant glacial phases. Note that the southern valley is much longer and gently dipping compared to the north. n.a.: not applicable.

$18.7^{-0.8}/_{-0.9}$ ka in the south and north, respectively. From the neighbouring Paring Mts, Urdea and Reuther (2009) reported five ^{10}Be CRE ages between 16.7 ± 1.5 and 17.9 ± 1.6 ka attributable to the M2 stage (not divided in sub-stages). Unfortunately, insufficient information regarding these sample sites and calculation of their CRE ages preclude the recalculation of these data. However, as the recalculation of the CRE ages of Reuther et al. (2007) provided ~16% older ages on average (Table S2), these ages likely belong to the M2a stage.

Due to the wide scatter of data from the boulderfield representing the next, M2b phase, its age of abandonment could be estimated at 16.9 ± 0.9 ka based on a single sample selected as representative on morphostratigraphic basis (see Section 4.1, Figs. 7, 8). The lack of convergence of the CRE durations is most probably the result of the long-lasting evolution and consequent transformation of the moraine complex into a wide boulderfield at the confluence of the two tributaries (Fig. 2). The age estimate of the M2b stage on the southern valleys of the Retezat Mts is in agreement with the $17.0^{+0.7}/_{-0.6}$ ka most probable CRE age of this phase on the northern slopes (Fig. 9).

The moraines of the subsequent M3a phase stabilized at $15.8^{+0.9}/_{-0.6}$ ka in the Bucura valley, while no age constraint is available in the north. The large number of old outliers in the next, M3b sample set suggests that a considerable part of the boulders transported by the glacier during this phase contains a non-negligible amount of inherited ^{10}Be (Fig. 7). The cluster of the four youngest samples was used for the determination of the most probable CRE age of this phase at $15.6^{+0.8}/_{-0.8}$ ka. Around this phase the glacier retreat apparently accelerated, as the M3a and M3b phases provided statistically indistinguishable most probable ages. The recalculated CRE age of the M3b phase is $15.5^{-0.7}/_{-0.8}$ ka in the northern valleys, which is in agreement with the timing of this phase in the south (Figs. 8, 9).

Several studies reported phases of rapid ice retreat, on the basis of indistinguishable ^{10}Be age populations (Goehring et al., 2008; Briner et al., 2009; Koester et al., 2017; Corbett et al., 2019). This is due to the fact that the precision of the CRN data (in this study 4–5% internal and 9–10% external uncertainty) is not good enough to distinguish between millennial scale climate events (Delmas et al., 2008; Balco, 2020).

The CRE ages of the dataset belonging to the last, M4 deglaciation phase, resulted to be largely scattered and mostly yielding old ages compared to the morphostratigraphic position of this landform (Fig. 6). This pattern, again, suggests the presence of certain amount of inheritance (Balco, 2020). Due to the lack of an age cluster in the widely scattered M4 dataset, the CRE age of the youngest sample, 14.4 ± 0.5 ka, was accepted as the best estimate for the time of abandonment of the moraines (Applegate et al., 2012). This age estimate is in agreement with the morphostratigraphic position of the M4 moraine, postdating the moraine of the M3b phase (Figs. 2, 6, 7, 9). This age estimate is similar to the recalculated most probable exposure age of $14.9^{+0.6}/_{-0.5}$ ka of a dated moraine on the north ($n = 2$; Ruszkiczay-Rüdiger et al., 2016).

The bedrock and boulder samples collected from the Berbecilor Cirque lay well above the M4 moraines, therefore they must have been abandoned by the receding glacier after the M4 phase. Conversely, the bedrock surfaces and boulders provided apparent exposure durations equivalent to the local M1 and M2a phases, when the glacier terminus was ~18 and ~6 km down-valley, respectively (Figs. 2, 6, 7, 8). The absence of moraines in higher positions within the cirques suggests that the fast glacier retreat recorded by the overlapping ages of the M3a and M3b moraines continued after the abandonment of the M4 moraines. Following this line of evidence, the complete deglaciation of the cirque area could have taken place within a few hundred years after the abandonment of the M4 moraines. Hence, the time of the deglaciation of the area was tentatively placed to ~14 ka.

In order to verify or reject the CRE age estimates of the M3b and M4 phases and also the timing of the deglaciation of the cirque area, the following section is dedicated to the study of independent regional and local paleoclimate data.

5.2. Independent data constraining the age of the last deglaciation of the Retezat Mts

In the Retezat Mts fast melting of the glaciers between ~16 and ~14 ka was suggested by overlapping CRE durations of the subsequent terminal moraine generations of the M3a, M3b and M4 glacial phases. The Greenland Ice Core Chronology (GICC) places the onset of the Greenland Interstadial-1 (GI-1, or Bölling/Alleröd interstadial) to this time, suggesting abrupt warming between ~14.7 and ~14.1 ka (GI-1e) (Rasmussen et al., 2014).

The chironomid-inferred mean July air temperature record at Lake Brazi (a lake within the M3a moraine in a northern valley of the Retezat Mts, Figs. 1, S2) suggests a warming of 2.8 °C between ~14.7 and ~14.5 ka cal BP, at the onset of the GI-1 (Tóth et al., 2012). This warming was also observable in the vegetation record, which indicates the expansion of forests from 14.5 ka cal BP in the Southern Carpathians (Magyari et al., 2011, 2012). The temperature signal of branched tetraether lipids from the NW Black Sea sediments indicates ~3 °C warming of the catchment at ~15.0–14.5 ka, and these warmer conditions continued between ~14.5 and ~13.5 ka (Sanchi et al., 2014). The warming between ~15 ka and ~14 ka indicated by these paleotemperature reconstructions suggest that this period was favourable for glacier melting in Southeast Europe.

The studies of the sediment sequences and age-depth modelling based on radiocarbon dating of two lakes behind the M3b moraines in the Retezat Mts yielded results comparable to the CRE dating of these landforms. In the northern Gales valley (Figs. 1, S2), the onset of lacustrine sedimentation was estimated at ~15.1 ka (Lake Gales; Magyari et al., 2009; Hubay et al., 2018), in agreement with the ~15.5 ka CRE age of the M3b moraines. Interestingly, in the southern Bucura valley the modelled onset of sediment deposition was ~17.1 ka (Lake Lia; Hubay et al., 2018), which seems to be much earlier than the age of deglaciation of that part of the valley. However, the bottom sequence of the studied core consisted of purely minerogenic silt fraction, most probably representing the fluvioglacial facies of fast deposition in front of the glacier tongue. Accordingly, it does not represent a lacustrine sedimentation. Regarding the modelled age of the depth level where silt dominated sediment changes to gyttja, which likely corresponds to the actual onset of lacustrine sedimentation in the Lia basin, an age of ~13.2 ka cal BP can be inferred from the published age-depth plot (Hubay et al., 2018), which is setting aside the contradiction with the ~15.6 ka CRE age of the M3b phase suggested by the present study.

Unfortunately, the sediment core of Lake Bucura, lying behind the moraine of the M4 phase, did not reach the bedrock. At a depth of 5 m, the age of the sediment was ~10.4 ka cal BP (Hubay et al., 2018), which can only be taken as a minimum age of the abandonment of the moraines of the M4 phase.

In summary, the CRE age suggested by the youngest sample cluster of the M3b moraines seems to be acceptable, and consequently devoid of considerable amount of inherited ^{10}Be. The abandonment of the last M4 moraine between ~15 and ~14 ka as well as the ~14 ka date for the final deglaciation of the cirque area are also supported by independent climate- and geochronological data. Similarly to the northern valleys of the Retezat Mts, the Jablanica Mt. in the Central Balkan Peninsula and the Bohemian Forest, no GS-1 (YD) glacial advance has been recorded in the study area, most probably due to the cold and dry climate conditions in these areas (Vočadlová et al., 2015; Ruszkiczay-Rüdiger et al., 2016, 2020). This finding suggests higher ELA than considered for the recent reconstruction of large-scale continental pattern of the ELA across Europe (Rea et al., 2020). The 14 ka age of deglaciation will therefore be taken as a working hypothesis for the calculation of the inherited ^{10}Be inventory and modelling of the glacial denudation. Naturally, an underestimation of the deglaciation age would generate higher inherited ^{10}Be concentrations and a smaller depth of glacial denudation than presented below.

5.3. Estimating the duration of glacier-covered and ice-free periods

The inherited nuclide inventory can be used for the calculation of the depth of glacial erosion and glacial erosion rate provided that the duration of the ice-cover can be estimated. Two modelling scenarios were implemented: (1) considering the last interglacial-glacial cycle only, supposing that during the penultimate glaciation the glacial erosion was deep enough to remove the total amount of inherited CRN; (2) considering the last two glacial cycles, to test the effect of the inheritance of previous exposures. In both models the interglacial conditions are supposed to be similar to present.

In order to find the most suitable threshold between ice-free and glacier-covered conditions in the study area, a combination of the speleothem growth periods in the relict caves situated in the cirque region (~2300 m asl) in the Făgăraş Mts (Tîrlă et al., 2020) and the benthic $\delta^{18}O$ record (Lisiecki and Raymo 2005) was used (Fig. 10C). Speleothem growth phases in these alpine caves were established by the kernel density estimate (Vermeesch, 2012) of the speleothem U-Th ages from the past 300 k years (Tîrlă et al., 2020). A reasonable threshold was found at 4.25‰ in the benthic $\delta^{18}O$ stack record above which ice-free conditions can be assumed in the Southern Carpathians, as indicated by the speleothem growth phases in the alpine karst of the area during former interglacial conditions of MIS 5 and MIS 7. Using this threshold, the glaciated periods were estimated at ~191–130 ka (MIS 6) and ~71–14 ka (MIS 4–2) and the ice-free periods at ~243–191 ka (MIS 7), ~130–71 ka (MIS 5) and ~14–0 ka (MIS 1) (Fig. 10). Barr et al. (2019) suggested that cirques in the British Isles (somewhat more northerly, but at lower elevations than the Retezat Mts) were ice-free for 52 ± 21 kyrs during the last ~120 ka. This number is in agreement within error with the 57 kyrs duration of the last glacial cover and 63 kyrs ice-free estimated by this study during the same period. Accordingly, the above defined intervals of glaciated and non-glaciated phases will be used for the modelling of the depth of glacial erosion and glacial erosion rate.

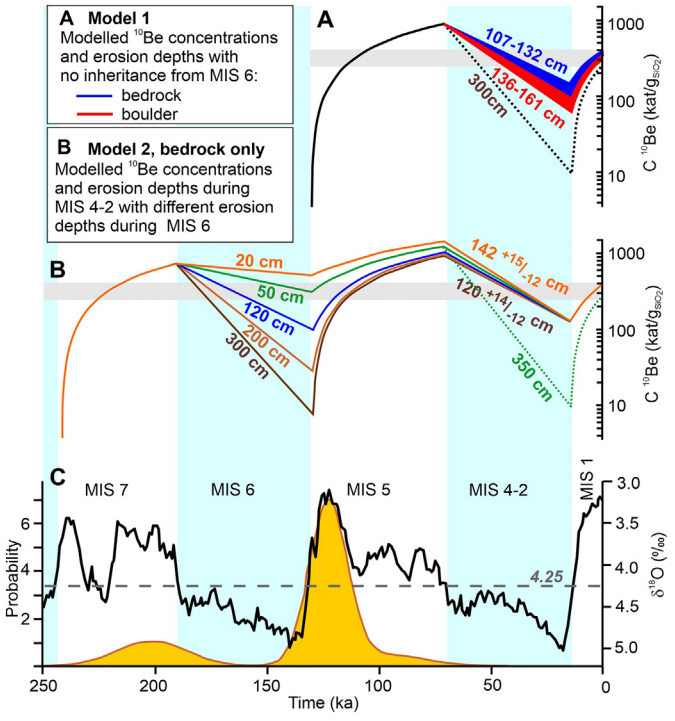

Fig. 10. A: The evolution of ^{10}Be concentrations and modelled depth of glacial erosion during the last glacial cycle in the bedrock (blue) and boulder (red) samples of the Berbecilor Cirque The cosmogenic clock was reset during the penultimate glacial cycle (Model 1). The dotted line indicates the 300 cm denudation depth, which is deep enough to reduce the inherited ^{10}Be inventory below detection limit for both boulders and bedrock. The grey shadow indicates the range between the ^{10}Be inventory produced in situ with no inheritance and the maximum measured value. B: The evolution of ^{10}Be concentrations and modelled depth of glacial erosion during the last glacial cycle for the bedrock surfaces. Different depths of glacial erosion during the penultimate glacial (MIS 6) are considered. The green dotted line shows the 350 cm denudation depth that is deep enough to reset the cosmogenic clock even if the denudation during the previous glaciation was as shallow as 50 cm. Fig. 12 shows the denudation rates modelled for both bedrock and boulder surfaces. C: The benthic $\delta^{18}O$ record and Marine Isotope Stages (Lisiecki and Raymo, 2005; solid black line) and kernel density estimate of speleothem U-Th age data from alpine caves in the Făgăraş Mts (Tîrlă et al., 2020; orange plot). The dashed line shows the $\delta^{18}O$ value of 4.25‰, which best fits both the U-Th speleothem data and the MIS stages. This threshold value is used to estimate the duration of unglaciated and glacier-covered periods in the study area (light blue shadows). For details refer to the text.

5.4. Quantification of the inherited CRN inventory and depth of glacial erosion in the cirque area

To estimate quantitatively the inherited cosmogenic ^{10}Be inventory, the bedrock and boulder samples from the Berbecilor Cirque were used (Tables 1, 2; Figs. 2, 3, 8). In order to assess the inherited ^{10}Be concentrations the ^{10}Be inventory produced in situ during the current exposure was calculated via Eq. (1) using the same correction factors as described in Section 3.3 (Tables S1, S2) and the presumed ~14 ka date of the deglaciation of the cirque area (Fig. 10). As a next step, this nuclide inventory was subtracted from the measured ^{10}Be concentration to get the inherited ^{10}Be inventory of (80.4 ± 3.1) × 10^3 at/g$_{SiO2}$ and (84.1 ± 3.3) × 10^3 at/g$_{SiO2}$ for the boulder samples and (133.6 ± 5.1) × 10^3 at/g$_{SiO2}$ and (116.1 ± 4.4) × 10^3 at/g$_{SiO2}$ for the bedrock surfaces (Fig. 11A).

This inherited component was produced at depth *z* during the penultimate exposure, which depth equals the depth of rock removed by glacial erosion (Fig. 11B). The depth *z* could be determined by inverse modelling via Eq. (1) using the above defined duration of the last interglacial as exposure duration (130–71 ka, 59 kyrs) and the same correction factors as for the recent exposure (described in Section 3.3).

In the simple model (1) considering only the last interglacial-glacial cycle, the inheritance (N_{inh} in Eq. (1)) was considered to be zero at the beginning of the last interglacial. For the bedrock surfaces on top of the stoss-and-lee landforms the depth of glacial erosion was between 117 ± 10 cm and 123 ± 9 cm (Re16-09 and Re16-13, respectively; 107–132 cm in total). For the boulders the denudation depth was somewhat larger, 150 ± 11 cm and 147 ± 11 cm (Re16-11 and Re16-12, respectively; 136–161 cm in total) (Figs. 10A and 11C). The model also demonstrated, that a denudation depth of ~300 cm would have been enough to reduce the inherited ^{10}Be concentrations below the detection limit (or within the uncertainties of the measured values after 14 ka exposure; Fig. 10A). In case of previous exposure durations and lower analytical uncertainties the glacial denudation necessary to remove the cosmogenic nuclides accumulated during previous exposures may be larger. For instance, in SW Norway glacial erosion of over 5 m was required to remove detectable traces of inherited ^{10}Be (Briner et al., 2016).

In model (2) the evolution of the ^{10}Be concentrations over time was examined for the last two interglacial-glacial cycles in order to trace the potential effect of the previous exposures on the modelled depth of glacial erosion. In this model, the depth of glacial denudation during the last (MIS 4-2) glacial was modelled with several erosion depths during the previous (MIS6) glacial (Figs. 10B, 12). The first observation is that even if the depth of glacial erosion was zero during the penultimate glacial, $179^{+15}/_{-11}$ cm and $149^{+15}/_{-12}$ cm glacial denudation is enough to reach the measured ^{10}Be concentrations in the boulder and bedrock surfaces, respectively. Then the thickness to be eroded during the last glacial is reduced with the increase of the erosion depth during the MIS 6. However, for erosion depths over 150 cm during the MIS 6, the change of the modelled erosion depth for the MIS 4-2 is minimal (around 150 for boulders and 120 cm for bedrock).

The depth of glacial erosion necessary to reset the cosmogenic clock during the last glaciation remains ~300 cm if at least ~100 cm of rock was eroded during the MIS 6, similarly to the single stage model (Fig. 10A, B). In case of the MIS 6 glacial erosion is shallower, the erosion

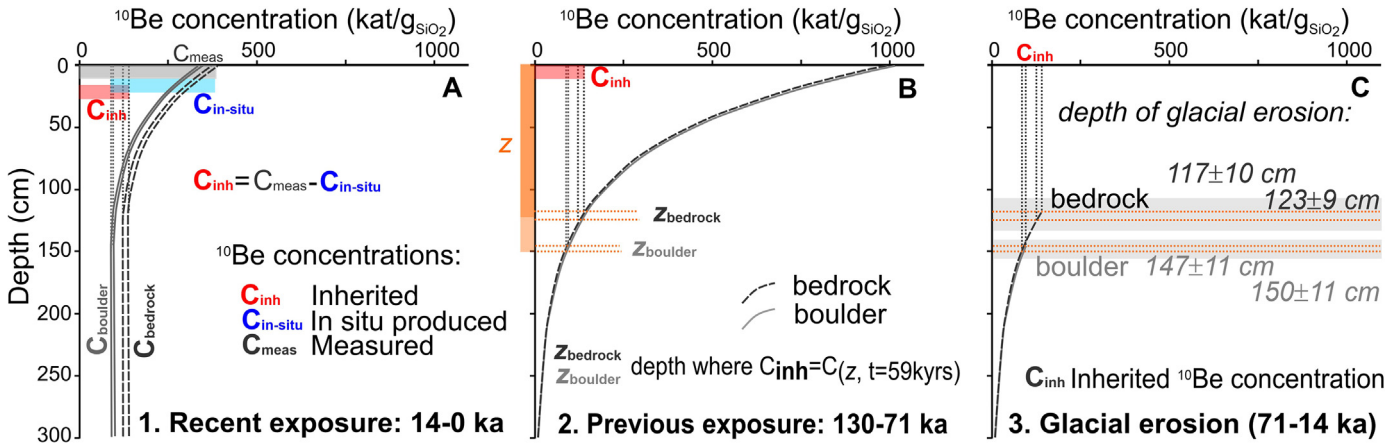

Fig. 11. The change of ^{10}Be concentrations with depth in the bedrock and boulder samples of the Berbecilor Cirque considering the last interglacial-glacial cycle. A: The change of ^{10}Be concentrations with depth during the recent exposure (MIS 1, 14–0 kyr) with the measured, inherited and in-situ produced ^{10}Be inventories indicated. B: The change of ^{10}Be concentrations with depth during the previous exposure (MIS 5, 130–71 ka). The calculated inherited amount of ^{10}Be is used to derive *z* depth of glacial erosion during the last glacial. C: The modelled depth of glacial erosion (*z*) (with uncertainties as grey shadows) as calculated using the inherited ^{10}Be concentrations (orange dotted lines, grey shadows show the uncertainties).

of at least ~350 cm of rock would be necessary during the MIS-4-2 to reduce the inherited CRN concentration under detection limit (Fig. 10B).

As it is well visible on Figs. 10A, B and 12 the depth of glacial erosion during the previous glaciation has a limited effect on the modelled glacial denudation depth during the last glaciation. The depth to be eroded to reduce the inherited cosmogenic nuclide inventory below detection limit is 300 to 350 cm. The measured ^{10}Be concentrations in bedrock and boulder surfaces is reached by $118^{+14}/_{-11}$ cm and $147^{+14}/_{-11}$ cm of glacial erosion in case of no inheritance, while this value is $149^{+15}/_{-12}$ cm and $179^{+15}/_{-11}$ cm for the extreme case of no erosion during the penultimate glaciation. Accordingly, the required increase of glacial erosion during the last glacial is up to 18–20% considering the two end-member scenarios: at least 4 m and zero denudation during the previous glaciation.

5.5. Spatial and temporal pattern of glacial denudation in the Retezat Mts

Following the same line of thought, the long-term average glacial denudation rate can be estimated using the depth of glacial erosion and the duration of the ice-covered period calculated above (Section 5.3, Fig. 10). The uneven and episodic nature of glacial erosion prevents this value from being suitable for the estimation of a constant glacial erosion rate (which contradicts the nature of glacial erosion) however, it can be useful for the data comparison from different time and geological settings.

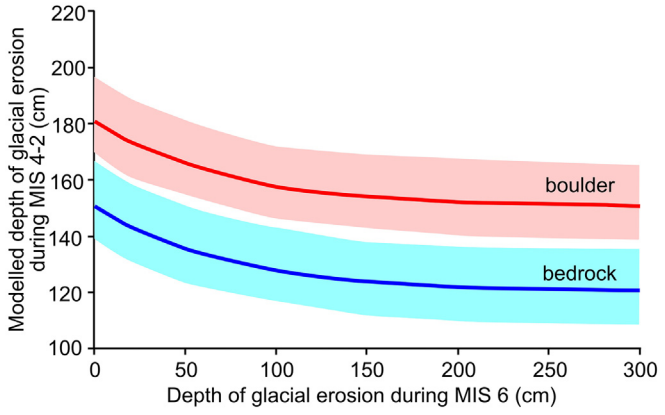

Fig. 12. Depth dependence of glacial erosion during the last (MIS 4-2) glaciation on the depth of glacial denudation during the previous (MIS 6) glaciation. Note that an erosion depths over 150 cm during the MIS 6, leads to minimal change of the modelled erosion depth during the MIS 4-2.

During the last glacial phase (MIS 4-2) in the Berbecilor Cirque of the Retezat Mts the mean glacial erosion rate was 20–24 mm/kyr and 25–29 mm/kyr for the bedrock and for the boulder samples, respectively, if the cosmogenic nuclide clock was successfully reset during the penultimate glacial phase. In case the rock thickness removed by the penultimate glaciation was not insufficient for the complete removal of the cosmogenic ^{10}Be inventory (Figs. 10B and 12) the glacial erosion rate can be estimated to 19–28 mm/kyr for bedrock and 24–33 mm/kyr for boulder surfaces. The boulders are mostly grabbed from the lee side of the stoss-and-lee landforms, where the glacial erosion and plucking is more efficient than on their top surfaces (Wirsig et al., 2017), which explains the somewhat larger estimated erosion rate for boulder samples.

By way of comparison, in the Făgăraş Mountains 600 mm/kyr has been suggested as the glacial erosion rate of a cirque based on cirque morphometry (Tîrlă et al., 2020). This value can be considered a maximum estimate, as the applied model supposed a single stage evolution of the cirque during the last glacial period (MIS 4-2) and ignored cirque evolution during previous glaciations. Briner and Swanson (1998) used in situ produced ^{36}Cl data also on stoss-and-lee landforms and boulders on Mt. Erie (Cordilleran Ice Sheet). They showed that less than 1–2 m of rock was removed by glacial erosion during the last glacial phase, which means glacial erosion rates of 90–350 mm/kyr. In the Eastern Pyrenees, Crest et al. (2017) observed that the ^{10}Be and ^{26}Al CRE ages of the cirque floors were older than the relevant moraine ages. They concluded that subglacial cirque-floor denudation rates were typically 0–120 mm/kyr (occasionally up to >300 mm/kyr). The glacial denudation rates estimated for the Berbecilor Cirque in the Retezat Mts are in the lower range of the reported values. Wirsig et al. (2017) described higher glacial denudation rates (from 100 mm/kyr to >5000 mm/kyr) from bedrock surfaces in the Eastern Alps however, over a considerably shorter, 700–3300 years timespan preceding the Little Ice Age. The higher values were estimated towards the centre of the glacial valley and on the leeward side of the bedrock knobs on the valley floor.

However, due to the already mentioned intermittent nature of glacial erosion, two main issues might complicate the comparison of published glacial erosion rates: the methodology and the time considered: i) according to a global review of glacial erosion rates, CRE dating provided systematically lower glacial denudation rates compared to other methods (Delmas et al., 2009); ii) the considered period of glacial erosion and its duration is also an important issue, and depend on the approach of whether to integrate the entire glacial phase or just a

restricted period (e.g. glacier expansion, maximum or recession). For instance, 2 m of erosion considered for a period of 10 kyrs or 60 kyrs makes a proportional difference for he estimated denudation rate (i.e. 200 mm/kyr or 33 mm/kyr).

The effect of the inheritance in the study area is striking in the upper part of the valleys, in other words, only landforms belonging to the last two glacial phases appear to be affected. Most probably, when the glaciers were more extensive, major part of the glacially transported material originated from lower elevations, where glacial erosion carved deeper into the valleys. This is in agreement with the suggestion that cirques grow mainly when glaciers are restricted to the cirque zone rather than during periods of extensive glaciation (Barr and Spagnolo, 2015). During full glacial periods, glacier erosion was focused on the lower sections of the glacial valley, leaving the cirque floors less affected by denudation. The main reasons for the limited glacial erosion in the cirques during the extended glacial phases might stem form cold-based and shallow, low-gradient glaciers (absence of rotational flow) in the cirques, coupled with glacier-load starvation (because permafrost drastically decreases the potential for clast supply) (Crest et al., 2017). In these conditions the ice is frozen to the underlying bedrock where stress (and basal shearing) reduces to zero. As a consequence, the ice-rock interface remains below the pressure melting point and overlying ice moves via internal plastic deformation only. Cold-based glaciers have been reported as the primary reason for the considerable amount of inherited ^{10}Be in the moraine boulders of small alpine and cirque glaciers in East Antarctica as well (Valletta et al., 2017).

As the glaciers retreat and the ELA is approaching the cirque area, the conditions switch to those favourable to glacial erosion: the shortened glaciers become steeper and their thermal regime changes to temperate (warm-based). In warm-based glaciers bedrock is eroded by the sliding basal ice, with temperatures above the pressure-melting point (Benn and Evans, 2010). Besides, the sediment supply may increase due to the warmer air temperature promoting frost cracking and thereby supplying more abrasive debris to the glacier (Barr et al., 2019). Contemporary glacial erosion rates, together with ice fluxes and sliding speeds for 15 outlet glaciers in Patagonia have shown that rising temperatures increase the erosive potential of glacial ice (Koppes et al., 2015). In the Retezat Mts however, the fast deglaciation of the upper valleys (in 1–3 kyrs) could not provide enough time to remove at least ~3 m of rock to zero the cosmogenic nuclide clock.

Barr et al. (2019) have suggested that continuous cirque growth during glacier occupation is unlikely, and proposed that cirques attained much of their size during the first occupation of a non-glacially sculpted landscape. During subsequent glacier occupations, cirque growth may have slowed considerably, with the highest rates of subglacial erosion focused during periods of cirque glaciation. Considering the well-developed glacial landscape observed in the Retezat Mts, coupled with the limited glacial erosion during the LGM suggested by the CRN inventories of the landforms of the cirque area, implies that glacial landscape of the Retezat Mts must have been formed in the course of at least two, or possibly more glacial phases. In the absence of numerical ages for glacial landforms older than LGM, this is the first evidence of pre-LGM glaciation of the Southern Carpathians.

6. Conclusions

i) Deglaciation chronology: The MIE in the Retezat Mts was synchronous with the LGM, which was followed by a fast glacier recession during the Lateglacial. These findings are closely matching the glacial chronologies published in the NW Carpathians (Engel et al., 2017; Makos et al., 2018). On the basis of the ^{10}Be CRE data the final deglaciation occurred around ~14 ka, a date supported by independent paleoclimate reconstructions. No evidence of a Younger Dryas (GS-1) glacial advance has been recorded in the study area so far, which finding will help to refine the large-scale continental pattern of the reconstructed ELA trend across Europe.

ii) Glacial erosion: the presence of inherited cosmogenic ^{10}Be in moraines, glacial boulders and bedrock samples of the cirque region hinders the age determination of the last and penultimate deglaciation phases. This nuclide inventory must have accumulated during exposure(s) prior to the last glaciation, which points to the limited erosional efficacy of cirque glaciers during the last glacial phase. Modelling of the depth of glacial erosion suggests that 1.1–1.8 m of rock was eroded by the glaciers from the cirque area, at a glacial erosion rate of 19–33 mm/kyr during the last glacial period (MIS 4-2). The absence of inherited ^{10}Be inventory from the lower/older moraine samples suggests that carving of the glacial troughs during the LGM and early Lateglacial periods was deep enough to remove the cosmogenic nuclides from previous exposures. During these phases of extended glaciation most probably the cirque region was conserved under cold-based ice. In future research where the studied paleo-glaciation might have been dominated by cold-based glaciers, careful evaluation of the possibility of insufficient erosion and an inherited CRN inventory is recommended.

iii) Landscape evolution: The limited glacial erosion in the cirques during the LGM suggests that the development of these landforms must have taken place during several subsequent glacial phases, providing an indirect piece of evidence for repeated Quaternary glaciations in the Retezat Mts. The apparent absence of pre-LGM landforms is most probably the consequence of LGM glaciers overriding the previous glacial features and/or the difficulty of recognising the severely eroded remnants of a possibly more extended previous glaciation in the lower valleys.

iv) Future tasks: The next step to provide a better estimate of the timing of the last deglaciation of the area will be the use of the short-lived in situ produced ^{14}C. The more precise age estimate of the final deglaciation will also enable, if necessary, the re-assessment of the depth of glacial erosion and glacial erosion rates.

Declaration of competing interest

The authors declare that they have no known competing financial interests or personal relationships that could have appeared to influence the work reported in this paper.

Acknowledgements

This research was funded by the National Research, Development and Innovation Office of Hungary grants 124807 and 119039 and co-financed by the European Regional Development Fund in the project of GINOP-2.3.2-15-2016-00009 'ICER'. New ^{10}Be measurements have been performed at the French AMS national facility ASTER (CEREGE, Aix en Provence) supported by the INSU/CNRS, the ANR through the "Projets thématiques d'excellence" program for the "Equipements d'excellence" ASTER-CEREGE action and IRD. We are grateful for Alexandru Hegyi for his help in sample collection, and for Máté Szabó for his contribution XRD measurement controlling the quality of purified quartz samples. We are grateful for the comments and suggestions of four Anonymous Reviewers, which helped to improve the manuscript.

This is contribution No.71. of 2 ka Palæoclimatology Research Group.

Appendix A. Supplementary data

Supplementary data associated with this article can be found in the online version, at https://doi.org/10.1016/j.geomorph.2021.107719. These data include the Google map of the most important areas described in this article.

References

André, M.F., 2002. Rates of postglacial rock weathering on glacially scoured outcrops (Abisko–Riksgränsen area, 68 N). Geogr. Ann. Ser. B 84 (3–4), 139–150.

Applegate, P.J., Urban, N.M., Keller, K., Lowell, T.V., Laabs, B.J., Kelly, M.A., Alley, R.B., 2012. Improved moraine age interpretations through explicit matching of geomorphic process models to cosmogenic nuclide measurements from single landforms. Quat. Res. 77 (2), 293–304.

Arnold, M., Merchel, S., Bourlès, D.L., Braucher, R., Benedetti, L., Finkel, R.C., Aumaître, G., Gottdang, A., Klein, M., 2010. The French accelerator mass spectrometry facility ASTER: improved performance and developments. Nucl. Instrum. Methods Phys. Res. B 268, 1954–1959.

Ayalon, A., Bar-Matthews, M., Frumkin, A., Matthews, A., 2013. Last Glacial warm events on Mount Hermon: the southern extension of the Alpine karst range of the east Mediterranean. Quat. Sci. Rev. 59, 43–56.

Balco, G., 2009. MATLAB Code for Camel Diagrams. http://cosmognosis.wordpress.com/2009/07/13/matlab-code-for-camel-diagrams (February 2013).

Balco, G., 2011. Contributions and unrealized potential contributions of cosmogenic-nuclide exposure dating to glacier chronology, 1990–2010. Quat. Sci. Rev. 30 (1–2), 3–27.

Balco, G., 2020. Glacier change and paleoclimate applications of cosmogenic-nuclide exposure dating. Annu. Rev. Earth Planet. Sci. 48, 21–48.

Balco, G., Stone, J.O., Lifton, N.A., Dunai, T.J., 2008. A complete and easily accessible means of calculating surface exposure ages or erosion rates from ^{10}Be and ^{26}Al measurements. Quat. Geochronol. 3, 174–195.

Barr, I.D., Spagnolo, M., 2015. Glacial cirques as palaeoenvironmental indicators: their potential and limitations. Earth Sci. Rev. 151, 48–78.

Barr, I.D., Ely, J.C., Spagnolo, M., Evans, I.S., Tomkins, M.D., 2019. The dynamics of mountain erosion: cirque growth slows as landscapes age. Earth Surf. Proc. Landf. 44 (13), 2628–2637.

Benn, D.I., Evans, D.J.A., 2010. Glaciers and Glaciation. Routledge, London, U.K., p. 817.

Berstad, I.M., Lundberg, J., Lauritzen, S.E., Linge, H.C., 2002. Comparison of the climate during marine isotope stage 9 and 11 inferred from a speleothem isotope record from Northern Norway. Quat. Res. 58 (3), 361–371.

Berza, T., Andar, P., Udrescu, C., Macalet, V., 1994. Retezat granitoid pluton (South Carpathians), a geochemical approach. Rom. J. Petrol. 76, 1–18.

Bierman, P.R., Marsella, K.A., Patterson, C., Davis, P.T., Caffee, M., 1999. Mid-Pleistocene cosmogenic minimum-age limits for pre-Wisconsinan glacial surfaces in southwestern Minnesota and southern Baffin Island: a multiple nuclide approach. Geomorphology 27 (1–2), 25–39.

Bierman, P.R., Davis, P.T., Corbett, L.B., Lifton, N.A., 2015. Cold-based, Laurentide ice covered new England's highest summits during the last glacial maximum. Geology 43, 1059–1062.

Borchers, B., Marrero, S., Balco, G., Caffee, M., Goehring, B., Lifton, N., Nishiizumi, K., Phillips, F., Schaefer, J., Stone, J., 2016. Geological calibration of spallation production rates in the CRONUS-Earth project. Quat. Geochronol. 31, 188–198.

Braucher, R., Brown, E.T., Bourlés, D.L., Colin, F., 2003. In situ produced ^{10}Be measurements at great depths: implications for production rates by fast muons. Earth Planet. Sci. Lett. 211, 251–258.

Braucher, R., Merchel, S., Borgomano, J., Bourles, D.L., 2011. Production of cosmogenic radionuclides at great depth: a multi element approach. Earth Planet. Sci. Lett. 309, 1–9.

Braucher, R., Guillou, V., Bourlès, D.L., Arnold, M., Aumaître, G., Keddadouche, K., Nottoli, E., 2015. Preparation of ASTER in-house ^{10}Be/^{9}Be standard solutions. Nucl. Instrum. Methods Phys. Res. Sect. B Beam Interact. Mater. At. 361, 335–340.

Briner, J.P., Swanson, T.W., 1998. Using inherited cosmogenic ^{36}Cl to constrain glacial erosion rates of the Cordilleran ice sheet. Geology 26 (1), 3–6.

Briner, J.P., Gosse, J.C., Bierman, P.R., 2006. Applications of cosmogenic nuclides to Laurentide Ice Sheet history and dynamics. Spec. Papers Geol. Soc. Am. 415, 29.

Briner, J.P., Bini, A.C., Anderson, R.S., 2009. Rapid early Holocene retreat of a Laurentide outlet glacier through an Arctic fjord. Nat. Geosci. 2, 496–499.

Briner, J.P., Goehring, B.M., Mangerud, J., Svendsen, J.I., 2016. The deep accumulation of ^{10}Be at Utsira, southwestern Norway: implications for cosmogenic nuclide exposure dating in peripheral ice sheet landscapes. Geophysical Res. Lett. 43 (17), 9121–9129.

Chmeleff, J., von Blanckenburg, F., Kossert, K., Jakob, D., 2010. Determination of the ^{10}Be half-life by multicollector ICP-MS and liquid scintillation counting. Nuclear Instrum. Methods Phys. Res. Sect. B Beam Interact. Mat. At. 268, 192–199.

Çiner, A., Stepišnik, U., Sarıkaya, M.A., Žebre, M., Yıldırım, C., 2019. Last Glacial Maximum and Younger Dryas piedmont glaciations in Blidinje, the Dinaric Mountains (Bosnia and Herzegovina): insights from ^{36}Cl cosmogenic dating. Medit. Geosci. Rev. 1 (1), 25–43.

Clark, D., Bierman, P., Larsen, P., 1995. Improving in situ cosmogenic chronometers. Quat. Res. 44, 367–377.

Codilean, A.T., 2006. Calculation of the cosmogenic nuclide production topographic shielding scaling factor for large areas using DEMs. Earth Surf. Process. Landf. 31 (6), 785–794.

Corbett, L.B., Bierman, P.R., Wright, S.F., Shakun, J.D., Davis, P.T., Goehring, B.M., Halsted, H. T., Koester, A.J., Cafee, M.W., Zimmerman, S.R., 2019. Analysis of multiple cosmogenic nuclides constrains Laurentide Ice Sheet history and process on Mt. Mansfield, Vermont's highest peak. Quat. Sci. Rev. 205, 234–246.

Crest, Y., Delmas, M., Braucher, R., Gunnell, Y., Calvet, M., Team, Aster, 2017. Cirques have growth spurts during deglacial and interglacial periods: evidence from ^{10}Be and ^{26}Al nuclide inventories in the central and eastern Pyrenees. Geomorphology 278, 60–77.

Delmas, M., Gunnell, Y., Braucher, R., Calvet, M., Bourlès, D., 2008. Exposure age chronology of the last glaciation in the eastern Pyrenees. Quat. Res. 69 (2), 231–241.

Delmas, M., Calvet, M., Gunnell, Y., 2009. Variability of Quaternary glacial erosion rates–a global perspective with special reference to the Eastern Pyrenees. Quat. Sci. Rev. 28 (5–6), 484–498.

Dumitrescu, A., Birsan, M.V., Nita, I.A., 2017. A Romanian daily high-resolution gridded dataset of snow depth (2005–2015). Geofizika 34 (2), 276–295.

Engel, Z., Braucher, R., Traczyk, A., Léanni, L., AsterTeam, 2014. ^{10}Be exposure age chronology of the last glaciation in the Krkonoše Mountains, Central Europe. Geomorphology 206, 107–121.

Engel, Z., Mentlík, P., Braucher, R., Minár, J., Léanni, L., 2015. Geomorphological evidence and ^{10}Be exposure ages for the Last Glacial Maximum and deglaciation of the Velká and Malá Studená dolina valleys in the High Tatra Mountains, central Europe. Quat. Sci. Rev. 124, 106–123.

Engel, Z., Mentlík, P., Braucher, R., Křížek, M., Pluháčková, M., Team, Aster, 2017. ^{10}Be exposure age chronology of the last glaciation of the Roháčská Valley in the Western Tatra Mountains, central Europe. Geomorphology 293, 130–142.

Evans, D., 2014. Glacial Landsystems. Routledge.

Fabel, D., Harbor, J., 1999. The use of in-situ produced cosmogenic radionuclides in glaciology and glacial geomorphology. Ann. Glaciol. 28, 103–110.

Fabel, D., Harbor, J., Dahms, D., James, A., Elmore, D., Horn, L., Daley, K., Steele, C., 2004. Spatial patterns of glacial erosion at a valley scale derived from terrestrial cosmogenic ^{10}Be and ^{26}Al concentrations in rock. Ann. Assoc. Am. Geogr. 94 (2), 241–255.

Florineth, D., Schlüchter, C., 1998. Reconstructing the Last Glacial Maximum (LGM) ice surface geometry and flowlines in the Central Swiss Alps. Eclogae Geol. Helv. 91, 391–407.

Gheorghiu, D., 2012. Testing Climate Synchronicity Since the Last Glacial Maximum Between Scotland and Romania. (PhD thesis). Univ. of Glasgow, p. 200.

Gheorghiu, D.M., Hosu, M., Corpade, C., Xu, S., 2015. Deglaciation constraints in the Parâng Mountains, Southern Romania, using surface exposure dating. Quat. Int. 388, 156–167.

Goehring, B.M., Brook, E.J., Linge, H., Raisbeck, G.M., Yiou, F., 2008. Beryllium-10 exposure ages of erratic boulders in southern Norway and implications for the history of the Fennoscandian Ice Sheet. Quat. Sci. Rev. 27, 320–336.

Goehring, B.M., Schaefer, J.M., Schluechter, C., Lifton, N.A., Finkel, R.C., Jull, A.T., Akçar, N., Alley, R.B., 2011. The Rhone Glacier was smaller than today for most of the Holocene. Geology 39 (7), 679–682.

Gosse, J.C., Phillips, F.M., 2001. Terrestrial in situ cosmogenic nuclides: theory and application. Quat. Sci. Rev. 20, 1475–1560.

Graf, A., Akçar, N., Ivy-Ochs, S., Strasky, S., Kubik, P.W., Christl, M., Burkhard, M., Wieler, R., Schlüchter, C., 2015. Multiple advances of Alpine glaciers into the Jura Mountains in the Northwestern Switzerland. Swiss J. Geosci. 108, 225–238.

Harrison, S., Glasser, N., Anderson, E., Ivy-Ochs, S., Kubik, P.W., 2010. Late Pleistocene mountain glacier response to North Atlantic climate change in southwest Ireland. Quat. Sci. Rev. 29 (27–28), 3948–3955.

Heisinger, B., Lal, D., Jull, A.T., Kubik, P., Ivy-Ochs, S., Neumaier, S., Knie, K., Lazarev, V., Nolte, E., 2002a. Production of selected cosmogenic radionuclides by muons: 1. Fast muons. Earth Planet. Sci. Lett. 200 (3–4), 345–355.

Heisinger, B., Lal, D., Jull, A.T., Kubik, P., Ivy-Ochs, S., Knie, K., Nolte, E., 2002b. Production of selected cosmogenic radionuclides by muons: 2. Capture of negative muons. Earth Planet. Sci. Lett. 200 (3–4), 357–369.

Heyman, J., Stroeven, A.P., Harbor, J.M., Caffee, M.W., 2011. Too young or too old: evaluating cosmogenic exposure dating based on an analysis of compiled boulder exposure ages. Earth Planet. Sci. Lett. 302 (1–2), 71–80.

Heyman, J., Applegate, P.J., Blomdin, R., Gribenski, N., Harbor, J.M., Stroeven, A.P., 2016. Boulder height–exposure age relationships from a global glacial ^{10}Be compilation. Quat. Geochronol. 34, 1–11.

Hippe, K., Ivy-Ochs, S., Kober, F., Zasadni, J., Wieler, R., Wacker, L., Kubik, P.W., Schlüchter, C., 2014. Chronology of Lateglacial ice flow reorganization and deglaciation in the Gotthard Pass area, Central Swiss Alps, based on cosmogenic ^{10}Be and in situ ^{14}C. Quat. Geochronol. 19, 14–26.

Hubay, K., Molnár, M., Orbán, I., Braun, M., Bíró, T., Magyari, E., 2018. Age–depth relationship and accumulation rates in four sediment sequences from the Retezat Mts, South Carpathians (Romania). Quat. Int. 477, 7–18.

Hugget, R.J., 2007. Glacial and glaciofluvial landscapes. Fundamentals of Geomorphology. Routledge Fundamentals of Phys. Geography, pp. 246–276.

Hughes, P.D., Woodward, J.C., van Calsteren, P.C., Thomas, L.E., Adamson, K., 2010. Pleistocene ice caps on the coastal mountains of the Adriatic Sea: palaeoclimatic and wider palaeoenvironmental implications. Quat. Sci. Rev. 29, 3690–3708.

Hughes, P.D., Gibbard, P.L., Woodward, J.C., 2005. Quaternary glacial records in mountain regions: a formal stratigraphical approach. Episodes-Newsmagazine of the International Union of Geol. Sci. 28 (2), 85–92.

Hughes, P.D., Woodward, J.C., van Calsteren, P.C., Thomas, L.E., 2011. The glacial history of the Dinaric Alps, Montenegro. Quat. Sci. Rev. 30, 3393–3412.

Hughes, P.D., Gibbard, P.L., Ehlers, J., 2013. Timing of glaciation during the last glacial cycle: evaluating the concept of a global 'Last Glacial Maximum' (LGM). Earth-Sci. Rev. 125, 171–198.

van Husen, D., 2004. Quaternary glaciations in Austria. In: Ehlers, J., Gibbard, P.L. (Eds.), Quaternary Glaciations—Extent and Chronology, Part I, pp. 1–13.

Ignéczi, Á., Nagy, B., 2016. Former plateau ice fields in the Godeanu Mountains, Southern Carpathians: first evidence of glaciated peneplains in the Carpathians. Quat. Int. 415, 74–85.

Isola, I., Ribolini, A., Zanchetta, G., Bini, M., Regattieri, E., Drysdale, R.N., Hellstrom, J.C., Bajo, P., Montagna, P., Pons-Branchu, E., 2019. Speleothem U/Th age constraints for the Last Glacial conditions in the Apuan Alps, northwestern Italy. Palaeogeogr. Palaeoclimat. Palaeoecol. 518, 62–71.

Ivy-Ochs, S., 2015. Glacier variations in the European Alps at the end of the last glaciation. Cuadernos Investig. Geogr. 41, 295–315.

Ivy-Ochs, S., Schäfer, J., Kubik, P.W., Synal, H.A., Schlüchter, C., 2004. Timing of deglaciation on the northern Alpine foreland (Switzerland). Eclogae Geol. Helv. 97 (1), 47–55.
Ivy-Ochs, S., Schlüchter, C., Kubik, P.W., Synal, H.-A., Beer, J., Kerschner, H., 1996. The exposure age of an Egesen moraine at Julier Pass, Switzerland, measured with cosmogenic radionuclides ^{10}Be, ^{26}Al and ^{36}Cl. Eclogae Geol. Helv. 89, 1049–1063.
Jansen, J.D., Knudsen, M.F., Andersen, J.L., Heyman, J., Egholm, D.L., 2019. Erosion rates in Fennoscandia during the past million years. Quat. Sci. Rev. 207, 37–48.
Kłapyta, P., Mîndrescu, M., Zasadni, J., 2020. Geomorphological record and equilibrium line altitude of glaciers during the last glacial maximum in the Rodna Mountains (eastern Carpathians). Quat. Res., 1–20 https://doi.org/10.1017/qua.2020.90.
Knudsen, M.F., Egholm, D.L., 2018. Constraining Quaternary ice covers and erosion rates using cosmogenic ^{26}Al/^{10}Be nuclide concentrations. Quat. Sci. Rev. 181, 65–75.
Koester, A.J., Shakun, J.D., Bierman, P.R., Davis, P.T., Corbett, L.B., Braun, D., Zimmerman, S.R., 2017. Rapid thinning of the Laurentide Ice Sheet in coastal Maine, USA, during late Heinrich Stadial 1. Quat. Sci. Rev. 163, 180–192.
Koppes, M., Hallet, B., Rignot, E., Mouginot, J., Smith Wellner, J., Boldt, K., 2015. Observed latitudinal variations in erosion as a function of glacier dynamics. Nature 526, 100103.
Korschinek, G., Bergmaier, A., Faestermann, T., Gerstmann, U.C., Knie, K., Rugel, G., Wallner, A., Dillmann, I., Dollinger, G., Lierse von Gostomski, Ch., Kossert, K., Maiti, M., Poutivtsev, M., Remmert, A., 2010. A new value for the half-life of ^{10}Be by heavy-ion elastic recoil detection and liquid scintillation counting. Nuclear Instrum. Methods Phys. Res. Sect. B Beam Interact. Mat. At. 268, 187–191.
Kuhlemann, J., Dobre, F., Urdea, P., Krumrei, I., Gachev, E., Kubik, P., Rahn, M., 2013. Last Glacial Maximum Glaciation of the Central South Carpathian Range (Romania). Aust. J. Earth Sci. 106, 83–95.
Kuhlemann, J., Milivojević, M., Krumrei, I., Kubik, P.W., 2009. Last glaciation of the Šara range (Balkan peninsula): increasing dryness from the LGM to the Holocene. Austrian J. Earth Sci. 102 (1), 146–158.
Lal, D., 1991. Cosmic ray labeling of erosion surfaces: in situ nuclide production rates and erosion models. Earth Planet. Sci. Lett. 104, 424–439.
Li, Y.K., 2013. Determining topographic shielding from digital elevation models for cosmogenic nuclide analysis: a GIS approach and field validation. J. Mt. Sci. 10 (3), 355–362.
Lifton, N.A., 2016. Implications of two Holocene time-dependent geomagnetic models for cosmogenic nuclide production rate scaling. Earth Planet. Sci. Lett. 433, 257–268.
Lifton, N.A., Sato, T., Dunai, T.J., 2014. Scaling in situ cosmogenic nuclide production rates using analytical approximations to atmospheric cosmic-ray fluxes. Earth Planet. Sci. Lett. 386, 149–160.
Lisiecki, L.E., Raymo, M.E., 2005. A Pliocene-Pleistocene stack of 57 globally distributed benthic δ^{18}O records. Paleoceanography 20 (1), PA1003. https://doi.org/10.1029/2004PA001071.
Lukas, S., 2006. Morphostratigraphic principles in glacier reconstruction-a perspective from the British Younger Dryas. Prog. Phys. Geogr. 30 (6), 719–736.
Magyari, E.K., Braun, M., Buczkó, K., Kern, Z., László, P., Hubay, K., Bálint, M., 2009. Radiocarbon chronology and basic characteristics of glacial lake sediments in the Retezat Mts (S Carpathians, Romania): a window to Lateglacial and Holocene climatic and palaeoenvironmental changes. Central Eur. Geol. 52, 225–248.
Magyari, E.K., Major, Á., Bálint, M., Nédli, J., Braun, M., Rácz, I., Parducci, L., 2011. Population dynamics and genetic changes of *Picea abies* in the South Carpathians revealed by pollen and ancient DNA analyses. BMC Evol. Biol. 11, 66.
Magyari, E.K., Jakab, G., Bálint, M., Kern, Z., Buczkó, K., Braun, M., 2012. Rapid vegetation response to Lateglacial and early Holocene climatic fluctuation in the South Carpathian Mountains (Romania). Quat. Sci. Rev. 35, 116–130.
Makos, M., Nitychoruk, J., Zreda, M., 2013a. Deglaciation chronology and paleoclimate of the Pięciu Stawów Polskich/Roztoki Valley, High Tatra Mountains, Western Carpathians since the Last Glacial Maximum, inferred from ^{36}Cl exposure dating and glacier–climate modeling. Quat. Int. 293, 63–78.
Makos, M., Nitychoruk, J., Zreda, M., 2013b. The Younger Dryas climatic conditions in the Za MnichemValley (Polish High Tatra Mountains) based on exposure-age dating and glacier–climate modeling. Boreas 42 (3), 745–761.
Makos, M., Dzierżek, J., Nitychoruk, J., Zreda, M., 2014. Timing of glacier advances and climate in the High Tatra Mountains (Western Carpathians) during the Last Glacial Maximum. Quat. Res. 82, 1–13.
Makos, M., Rinterknecht, V., Braucher, R., Żarnowski, M., ASTER Team, 2016. Glacial chronology and palaeoclimate in the Bystra catchment, Western Tatra Mountains (Poland) during the Late Pleistocene. Quat. Sci. Rev. 134, 74–91.
Makos, M., Rinterknecht, V., Braucher, R., Tołoczko-Pasek, A., ASTER Team, 2018. Last Glacial Maximum and Lateglacial in the Polish High Tatra Mountains-revised deglaciation chronology based on the ^{10}Be exposure age dating. Quat. Sci. Rev. 187, 130–156.
Margreth, A., Gosse, J.C., Dyke, A.S., 2016. Quantification of subaerial and episodic subglacial erosion rates on high latitude upland plateaus: Cumberland Peninsula, Baffin Island, Arctic Canada. Quat. Sci. Rev. 133, 108–129.
Marrero, S.M., Phillips, F.M., Borchers, B., Lifton, N., Aumer, R., Balco, G., 2016. Cosmogenic nuclide systematics and the CRONUScalc program. Quat. Geochronol. 31, 160–187.
Martin, L.C.P., Blard, P.-H., Balco, G., Lavé, J., Delunel, R., Lifton, N., Laurent, V., 2017. The CREp program and the ICE-D production rate calibration database: a fully parameterizable and updated online tool to compute cosmic-ray exposure ages. Quat. Geochronol. 38, 25–49.
Mațenco, L., 2017. Tectonics and exhumation of Romanian Carpathians: inferences from kinematic and thermochronological studies. In: Radoane, M., Vespremeanu-Stroe, A. (Eds.), Landform Dynamics and Evolution in Romania II. Springer Geography, pp. 15–56.
McDermott, F., 2004. Palaeo-climate reconstruction from stable isotope variations in speleothems: a review. Quat. Sci. Rev. 23 (7–8), 901–918.
Mentlík, P., Engel, Z., Braucher, T., Léanni, L., Aster Team, 2013. Chronology of the Late Weichselian glaciation in the Bohemian Forest in Central Europe. Quat. Sci. Rev. 65, 120–128.
Merchel, S., Herpers, U., 1999. An update on radiochemical separation techniques for the determination of long-lived radionuclides via accelerator mass spectrometry. Radiochim. Acta 84, 215–219.
Merchel, S., Gärtner, A., Beutner, S., Bookhagen, B., Chabilan, A., 2019. Attempts to understand potential deficiencies in chemical procedures for AMS: cleaning and dissolving quartz for ^{10}Be and ^{26}Al analysis. Nucl. Instr. Methods Phys. Res. B Beam Interact. Mat. At. 455, 293–299.
Micu, D., 2009. Snow pack in the Romanian Carpathians under changing climatic conditions. Meteorog. Atmos. Phys. 105, 1–16.
Micu, D.M., Dumitrescu, A., Cheval, S., Birsan, M.V., 2015. Climate of the Romanian Carpathians. Springer Int. Publ., p. 213.
Mîndrescu, M., Evans, I.S., Cox, N.J., 2010. Climatic implications of cirque distribution in the Romanian Carpathians: palaeowind directions during glacial periods. J. Quat. Sci. 25 (6), 875–888.
Niculescu, G., 1965. Munţii Godeanu: studiu geomorfologic. Editura Academiei Republicii populare Române, Bucuresti p. 339.
Popescu, R., Urdea, P., Vespermeanu-Stroe, A., 2017. Deglaciation history of high massifs from the Romanian Carpathians: towards an integrated view. In: Radoane, M., Vespremeanu-Stroe, A. (Eds.), Landform Dynamics and Evolution in Romania II. Springer Geography, pp. 87–116.
Prud'homme, C., Vassallo, R., Crouzet, C., Carcaillet, J., Mugnier, J.L., Cortés Aranda, J., 2020. Paired ^{10}Be sampling of polished bedrock and erratic boulders to improve dating of glacial landforms: an example from the Western Alps. Earth Surf. Proc. Landf. 45, 1168–1180.
Rasmussen, S.O., Andersen, K.K., Svensson, A.M., Steffensen, J.P., Vinther, B.M., Clausen, H.B., Siggaard-Andersen, M.-L., Johnsen, S.J., Larsen, L.B., Dahl-Jensen, D., Bigler, M., Röthlisberger, R., Fischer, H., Goto-Azuma, K., Hansson, M.E., Ruth, U., 2006. A new Greenland ice core chronology for the last glacial termination. J. Geophys. Res. 111, D06102.
Rasmussen, S.O., Bigler, M., Blockley, S.P.E., Blunier, T., Buchardt, S.L., Clausen, H.B., Cvijanovic, I., Dahl-Jensen, D., Johnsen, S.J., Fischer, H., Gkinis, V., Guillevic, M., Hoek, W.Z., Lowe, J.J., Pedro, J., Popp, T., Seierstad, I.K., Steffensen, J.P., Svensson, A.M., Vallelonga, P., Vinther, B.M., Walker, M.J.C., Wheatley, J.J., Winstrup, M., 2014. A stratigraphic framework for naming and robust correlation of abrupt climatic changes during the last glacial period based on three synchronized Greenland ice core records. Quat. Sci. Rev. 106, 14–28.
Rea, B.R., Pellitero, R., Spagnolo, M., Hughes, P., Ivy-Ochs, S., Renssen, H., Ribolini, A., Bakke, J., Lukas, S., Braithwaite, R.J., 2020. Atmospheric circulation over Europe during the Younger Dryas. Sci. Adv. 6 (50), eaba4844.
Reuther, A., Urdea, P., Geiger, C., Ivy-Ochs, S., Niller, H.P., Kubik, P., Heine, K., 2007. Late Pleistocene glacial chronology of the Pietrele Valley Retezat Mountains, Southern Carpathians, constrained by ^{10}Be exposure ages and pedological investigations. Quat. Int. 164, 151–169.
Rinterknecht, V., Matoshko, A., Gorokhovich, Y., Fabel, D., Xu, S., 2012. Expression of the Younger Dryas cold event in the Carpathian Mountains, Ukraine? Quat. Sci. Rev. 39, 106–114.
Ruszkiczay-Rüdiger, Zs, Kern, Z., Urdea, P., Braucher, R., Madarász, B., Schimmelpfennig, I., Team, A.S.T.E.R., 2016. Revised deglaciation history of the Pietrele-Stânişoara glacial complex, Retezat Mts, Southern Carpathians, Romania. Quat. Int. 415, 216–229.
Ruszkiczay-Rüdiger, Zs, Madarász, B., Kern, Z., Urdea, P., Braucher, R., Team, A.S.T.E.R., 2018. Glacier reconstruction, deglaciation chronology and paleo-environment reconstruction, Retezat Mountains, Southern Carpathians, Romania. Geologica Balcanica; Abstracts of the XXI. CBGA Congress, Salzburg, 10–13. September, 2018, pp. 240–241.
Ruszkiczay-Rüdiger, Z., Kern, Z., Temovski, M., Madarász, B., Milevski, I., Braucher, R., ASTER Team, 2020. Last deglaciation in the central Balkan Peninsula: geochronological evidence from the Jablanica Mt. (North Macedonia). Geomorphology 351, 106985.
Salcher, B.C., Starnberger, R., Götz, J., 2015. The last and penultimate glaciation in the North Alpine Foreland: New stratigraphical and chronological data from the Salzach glacier. Quat. Int. 388, 218–231.
Sanchi, L., Ménot, G., Bard, E., 2014. Insights into continental temperatures in the northwestern Black Sea area during the Last Glacial period using branched tetraether lipids. Quat. Sci. Rev. 84, 98–108.
Sarıkaya, M.A., Stepišnik, U., Žebre, M., Çiner, A., Yıldırım, C., Vlahović, I., Tomljenović, B., Matos, B., Wilcken, K.M., 2020. Last glacial maximum deglaciation of the Southern Velebit Mt.(Croatia): insights from cosmogenic ^{36}Cl dating of Rujanska Kosa. Mediterranean Geosci. Rev. 1–12.
Schaefer, J.M., Finkel, R.C., Balco, G., Alley, R.B., Caffee, M.W., Briner, J.P., Young, N.E., Gow, A.J., Schwartz, R., 2016. Greenland was nearly ice-free for extended periods during the Pleistocene. Nature 540 (7632), 252–255.
Shakun, J.D., Carlson, A.E., 2010. A global perspective on Last Glacial Maximum to Holocene climate change. Quat. Sci. Rev. 29, 1801–1816.
Shakun, J.D., Clark, P.U., He, F., Lifton, N.A., Liu, Z., Otto-Bliesner, B.L., 2015. Regional and global forcing of glacier retreat during the last deglaciation. Nat. Commun. 6 (1), 1–7.
Spötl, C., Mangini, A., 2007. Speleothems and paleoglaciers. Earth Planet. Sci. Lett. 254 (3–4), 323–331.
Stoll, H.M., Moreno, A., Mendez-Vicente, A., Gonzalez-Lemos, S., Jimenez-Sanchez, M., Dominguez-Cuesta, M.J., Edwards, R.L., Cheng, H., Wang, X., 2013. Paleoclimate and growth rates of speleothems in the northwestern Iberian Peninsula over the last two glacial cycles. Quat. Res. 80 (2), 284–290.
Stone, J.O., 2000. Air pressure and cosmogenic isotope production. J. Geophys. Res. 105 (B10), 23753–23759.

Stroeven, A.P., Fabel, D., Hättestrand, C., Harbor, J., 2002. A relict landscape in the centre of Fennoscandian glaciation: cosmogenic radionuclide evidence of tors preserved through multiple glacial cycles. Geomorphology 44 (1–2), 145–154.
Tîrlă, L., Drăguşin, V., Bajo, P., Covaliov, S., Cruceru, N., Ersek, V., Hanganu, D., Hellstrom, J., Hoffmann, D., Mirea, I., Sava, T., Sava, G., Şandric, I., 2020. Quaternary environmental evolution in the South Carpathians reconstructed from glaciokarst geomorphology and sedimentary archives. Geomorphology 354, 107038.
Tóth, M., Magyari, E.K., Brooks, S.J., Braun, M., Buczkó, K., Bálint, M., Heiri, O., 2012. A chironomid-based reconstruction of late glacial summer temperatures in the southern Carpathians (Romania). Quat. Res. 77, 122–131.
Urdea, P., 2000. Muntii Retezat. Studiu geomorphologic. Editura Academiei, Bucuresti, p. 272.
Urdea, P., 2004. The Pleistocene glaciation of the Romanian Carpathians. In: Ehlers, J., Gibbard, P.L. (Eds.), Quaternary Glaciations—Extent and Chronology, Part I, pp. 301–308.
Urdea, P., Reuther, A., 2009. Some new data concerning the Quaternary glaciation in the Romanian Carpathians. Geogr. Pannonica 13 (2), 41–52.
Urdea, P., Onaca, A., Ardelean, F., Ardelean, M., 2011. New Evidence on the Quaternary Glaciation in the Romanian Carpathians. Developments in Quaternary ScienceElsevier, Amsterdam, pp. 305–322.
Valletta, R.D., Willenbring, J.K., Lewis, A.R., 2017. "Difference dating": a novel approach towards dating alpine glacial moraines. Quat. Geochronol. 41, 1–10.
Vermeesch, P., 2007. CosmoCalc: an Excel add-in for cosmogenic nuclide calculations. Geochem. Geophys. Geosyst. 8, Q08003.
Vermeesch, P., 2012. On the visualisation of detrital age distributions. Chem. Geol. 312, 190–194.
Vočadlová, K., Petr, L., Žáčková, P., Křížek, M., Křížová, L., Hutchinson, S.M., Šobr, M., 2015. The Lateglacial and Holocene in Central Europe: a multi-proxy environmental record from the Bohemian Forest, Czech Republic. Boreas 44 (4), 769–784.
Voiculescu, M., Ardelean, F., 2012. Snow avalanche–disturbance of high mountain environment. Case study–the Doamnei glacial valley the Făgăraş massif-Southern Carpathians, Romanian Carpathians. Carpathian J. Earth Environ. Sci. 7 (1), 95–108.
Wirsig, C., Zasadni, J., Ivy-Ochs, S., Christl, M., Kober, F., Schlüchter, C., 2016. A deglaciation model of the Oberhasli, Switzerland. J. Quat. Sci. 31 (1), 46–59.
Wirsig, C., Ivy-Ochs, S., Reitner, J.M., Christl, M., Vockenhuber, C., Bichler, M., Reindl, M., 2017. Subglacial abrasion rates at Goldbergkees, Hohe Tauern, Austria, determined from cosmogenic ^{10}Be and ^{36}Cl concentrations. Earth Surf. Proc. Landf. 42 (7), 1119–1131.
Young, N.E., Lamp, J., Koffman, T., Briner, J.P., Schaefer, J., Gjermundsen, E.F., Linge, H., Zimmerman, S., Guilderson, T., Fabel, D., Hormes, A., 2018. Deglaciation of coastal south-western Spitsbergen dated with in situ cosmogenic ^{10}Be and ^{14}C measurements. J. Quat. Sci. 33 (7), 763–776.
Zasadni, J., Kłapyta, P., 2016. From valley to marginal glaciation in alpine-type relief: late glacial glacier advances in the Pieć Stawów Polskich/Roztoka Valley, High Tatra Mountains, Poland. Geomorphology 253, 406–424.
Zasadni, J., Kłapyta, P., Broś, E., Ivy-Ochs, S., Świąder, A., Christl, M., Balážovičová, L., 2020. Latest Pleistocene glacier advances and post-Younger Dryas rock glacier stabilization in the Mt. Kriváň group, High Tatra Mountains, Slovakia. Geomorphology 358, 107093.
Zugrăvescu, D., Polonic, G., Horomnea, M., Dragomir, V., 1998. Recent vertical crustal movements on the Romanian territory, major tectonic compartments and their relative dynamics. Rev. Roum. Geophys. 42, 3–14.